A digital twin approach for maritime carbon intensity evaluation accounting for operational and environmental uncertainty

Vasilikis, Nikolaos; Geertsma, Rinze; Coraddu, Andrea

DOI
10.1016/j.oceaneng.2023.115927

Publication date
2023

Document Version
Final published version

Published in
Ocean Engineering

Citation (APA)
Vasilikis, N., Geertsma, R., & Coraddu, A. (2023). A digital twin approach for maritime carbon intensity evaluation accounting for operational and environmental uncertainty. *Ocean Engineering*, *288*, Article 115927. https://doi.org/10.1016/j.oceaneng.2023.115927

Ocean Engineering 288 (2023) 115927

Contents lists available at ScienceDirect

Ocean Engineering

journal homepage: www.elsevier.com/locate/oceaneng

A digital twin approach for maritime carbon intensity evaluation accounting for operational and environmental uncertainty

Nikolaos Vasilikis [a], Rinze Geertsma [b,a], Andrea Coraddu [a,b,*]

[a] Department of Maritime & Transport Technology, Delft University of Technology, The Netherlands
[b] Faculty of Military Sciences, Netherlands Defence Academy, The Netherlands

ARTICLE INFO

Keywords:
Digital twin
Carbon intensity
Operational uncertainties
Environmental uncertainties
Data-driven methods
Hybrid propulsion

ABSTRACT

Maritime industry has set ambitious goals to drastically reduce its greenhouse gas emissions through stipulating and enforcing a number of energy assessment measures. Unfortunately, measures like the EEDI, EEXI, SEEMP and CII do not account for the operational and environmental uncertainty of operations at sea, even though they do provide a first means of evaluating the carbon footprint of ships. The increasing availability of high-frequency operational data offers the opportunity to quantify and account for this uncertainty in energy performance predictions. Current methods to evaluate and predict energy performance at a whole energy system level do not sufficiently account for operational and environmental uncertainty. In this work, we propose a digital twin that accurately predicts the fuel consumption and carbon footprint of the hybrid propulsion system of an Ocean-going Patrol Vessel (OPV) of the Royal Netherlands Navy under the aggregate effect of operational and environmental uncertainty. It combines first-principle steady-state models with machine learning algorithms to reach an accuracy of less than 5% MAPE on both mechanical and electrical propulsion, while bringing a 40% to 50% improvement over a model that does not utilise machine learning algorithms. Results over actual voyage intervals indicate a prediction accuracy of consumed fuel and carbon intensity within 2.5% accounting for a confidence interval of 95%. Finally, the direct comparison between mechanical and electrical propulsion showed no clear energy-saving benefits and a strong dependency of the results on each voyage's specific operational and environmental conditions.

1. Introduction

Human influence has unequivocally warmed the atmosphere and oceans, and the current speed of climate change and its impact on the living environment for mankind is unprecedented (IPCC, 2021). To reduce the impact of shipping on the environment, the International Maritime Organization (IMO) adopted mandatory energy efficiency measures already back in 2011 (MEPC, 2011). However, adopting these measures did not prevent a further 9.6% increase of green house gas emissions from shipping between 2012 and 2018 (IMO, 2020). Therefore, additional measures are urgently needed to reach a 40% reduction of carbon emissions per transport work by 2030 compared to 2008 (MEPC, 2018).

Literature provides a wide range of technological and operational solutions to comply with these measures (Vergara et al., 2012; Bouman et al., 2017; Damerius et al., 2022; Tadros et al., 2022). The main difficulty in their energy performance assessment, though, is the high uncertainty level of the required power for propulsion, mission, and auxiliary loads at the different design and operational phases (Georgescu et al., 2018; Vrijdag, 2014; Tillig et al., 2018; Vrijdag et al., 2018). This uncertainty is mainly caused by the heterogeneous operational and environmental conditions ships operate in, as demonstrated by Parkes et al. (2018) for merchant vessels and by Vasilikis et al. (2022) for multi-function service vessels.

Current IMO regulations and regulations in preparation by international authorities such as IMO and the European Union require ships to comply with reference limits of indices and indicators that, in principle, indicate the amount of carbon dioxide (CO_2) emissions per transport work. Their calculation is done either on a single sailing point as in the case of EEDI (MEPC, 2014) and EEXI (MEPC, 2021a) or by averaging the carbon footprint over a year of operations as in the case of CII (MEPC, 2021b). However, Lindstad et al. (2019) demonstrated that one sailing point does not consider the operational and environmental uncertainty at sea. Moreover, balancing out the effect of this uncertainty over the course of similar voyages does not provide

* Corresponding author at: Delft University of Technology, Faculty of Mechanical Engineering (previously 3mE), Building 34, Mekelweg 2, 2628CD Delft, The Netherlands.
E-mail addresses: n.vasilikis@tudelft.nl (N. Vasilikis), r.d.geertsma@tudelft.nl (R. Geertsma), a.coraddu@tudelft.nl (A. Coraddu).

https://doi.org/10.1016/j.oceaneng.2023.115927
Received 26 May 2023; Received in revised form 21 August 2023; Accepted 25 September 2023
Available online 7 October 2023

substantial feedback on the operational and design decisions, especially in the case of multi-function vessels that do not perform the same type of operations over time (Vasilikis et al., 2022). Therefore, this work aims at developing a digital twin that accounts for both operational uncertainty and unpredictability in environmental conditions.

The use of actual operating profiles or multiple operating conditions can improve the accuracy of the assessment of lifetime energy savings when comparing the impact of novel operational procedures and energy efficiency measures or design solutions (Trivyza et al., 2020; Gypa et al., 2023; Diez et al., 2018). The advent of new technological advances in collecting, storing, and transferring data has the potential to support the maritime industry to evaluate operational and design measures over more realistic operating conditions (Trodden et al., 2015; Nikolopoulos and Boulougouris, 2020). The increasing availability of high frequency operational data in contrast to bias-sensitive noon reports and research on data-driven techniques makes it possible to quantify operational and environmental uncertainties and accurately assess the energy efficiency of real-time operations (Aldous et al., 2015). In this work, we thus provide a novel methodology to account for realistic operating conditions in evaluating operational procedures, leveraging digital twin technologies that utilise high frequency operational data.

1.1. Related work

Uncertainties in operational and environmental conditions significantly affect the energy efficiency of power and propulsion systems (Baldi et al., 2015b; Esmailian et al., 2022). Operational uncertainty is the result of differences in loading condition, rudder activity, hull, and propeller fouling, but also of the selected vessel speed and acceleration. Alternatively, environmental uncertainty is mainly related to wind and wave conditions, currents, and ambient air and sea temperatures. Many authors account for those uncertainties differently by formulating their problem accordingly.

Some studies examine the efficiency of the whole energy conversion chain of ships' power supply and propulsion systems. Shi et al. (2010) and Sui et al. (2019) evaluate fuel consumption over the whole vessel speed range, accounting for one resistance curve that is assumed representative of the ship's operation. Other studies provide results for multiple resistance curves in order to demonstrate the effect of different weather and hull fouling conditions (Geertsma et al., 2017, 2018). Another practice is to provide the total fuel consumed over certain sailing time periods. For example, Sui et al. (2020) estimated energy gains over three voyages that each involved three parts of different sailing speeds and sea margins and a number of manoeuvres. Moreover, Trivyza et al. (2018, 2020) used actual vessel speed distributions, and finally, some authors examined actual vessel speed time profiles for energy management applications (Zhu et al., 2018; Kalikatzarakis et al., 2018). While these approaches partly consider the effect of diverse conditions on system-level energy performance with multiple single-point conditions, they do not account for the full spread of actual conditions.

Another set of studies focuses on individual operational and environmental parameters. They usually use hindcast data of monitored weather, vessel speed, and loading parameters. The main applications are on weather routing problems (Avgouleas and Sclavounos, 2014; Zhang et al., 2019; Zis et al., 2020), on operational parameters optimisation as trim (Coraddu et al., 2017) and vessel speed (Farag and Ölçer, 2020), but also on identifying hull fouling (Coraddu et al., 2019). Monte Carlo simulations have also been used to quantify uncertainty on attained energy efficiency (Coraddu et al., 2014; Fan et al., 2020). Furthermore, there is a third branch of studies that examine the energy performance of individual components and subsystems. They use statistical distributions of the main engine, auxiliary engine, and thermal power for thermodynamic cycle optimisation (Baldi et al., 2015a,b; Shu et al., 2017) or a number of typical steady state operating conditions (Sakalis and Frangopoulos, 2018). A similar strategy uses these power profiles in the time domain to examine different system configurations (Dedes et al., 2012, 2016; Ancona et al., 2018). The work proposed in this paper differs from these studies as it examines the aggregate effect of different operational and environmental conditions over selected voyages of the complete energy system rather than each parameter or subsystem separately.

Fuel consumption prediction of ships usually requires the development and use of simulation models of their energy systems (Moreno-Gutiérrez et al., 2015; Bulten, 2016). Literature provides many examples of such models, which usually consider different system limits and fidelity level. In general, simulation models can be categorised into first-principle models, that provide insight in the underlying physical processes, semi-empirical models, that use the experience of similar systems, and empirical models, that are built using the preceding

Table 1
Acronyms and symbols.

Acronyms	Description
EEDI	Energy efficiency design index
EEXI	Energy efficiency existing ship index
CII	Carbon intensity indicator
CI	Carbon intensity of a voyage interval
SEEMP	Ship energy efficiency management plan
IPMS	Integrated platform monitoring system
DT	Digital twin
MM	Mechanical mode
EM	Electrical mode
MDE	Main diesel engine
M	Electrical motor
DGEN	Diesel generator
PSH	Propeller shaft
CPP	Controllable pitch propeller
GB	Gearbox
MAE	Mean average error
MAPE	Mean absolute percentage error
APE	Absolute percentage error
REP	Relative error percentage
MS	Model selection
EE	Error estimation
RF	Random forest
SVR	Support vector regression
MLP	Multilayer perceptron network
RLS	Regularised least square
Symbols	**Description**
v	Vessel speed
v_a	Speed in the ship's wake
w	Taylor's wake factor
T_p	Propeller thrust
p	Propeller pitch
p_{nom}	Nominal propeller pitch
p_0	Zero-thrust propeller pitch
D	Propeller diameter
n	Propeller shaft speed
n_e	Main diesel engine speed
n_m	Electrical motor speed
r_e	Reduction ratio of main diesel engine
r_m	Reduction ratio of electrical motor
M_{psh}	Propeller shaft torque
P_{psh}	Propeller shaft power
P_m	Power provided by the electrical motors
$P_{m,el}$	Electrical power provided to the motors
P_e	Main diesel engine power
P_{gen}	Generated electrical power
P_{hotel}	Hotel electrical power
$\dot{m}_{f,e}$	Main diesel engines fuel consumption
$\dot{m}_{f,gen}$	Diesel generators fuel consumption
$\dot{m}_{f,tot}$	Total fuel consumption
T_{air}	Ambient air temperature
ρ	Sea water density
$M_{f,tot}$	Amount of fuel consumed on a voyage interval
Δt	Duration of a voyage interval
Δs	Distance of a voyage interval
$\bar{v}$	Average speed of a voyage interval

knowledge of the examined system's operation. Another way to categorise different models is a division into dynamic and steady-state models, based on whether they consider dynamic phenomena or not. Finally, simulation models can also be categorised into stochastic and deterministic models, depending on whether they consider the uncertainty of the input and output parameters or not. The application scope determines what would be a suitable model type and what should be the necessary fidelity level.

This trade-off between model type, application scope, and fidelity level has been discussed by many authors (Baldi, 2016; Geertsma et al., 2018; Sui et al., 2019). Energy performance prediction of ship energy systems usually utilises steady state models (Shi et al., 2010; Trivyza et al., 2018, 2020; Sui et al., 2019, 2020; Zhu et al., 2018). This is a practice followed in automotive applications as well (Barsali et al., 2004; Zuurendok, 2005; Zhou et al., 2016). Those models usually consist of two or three-dimensional look-up tables provided by component manufacturers or they are the result of regression analysis over a certain amount of available data. Some models use constant energy efficiencies to model different components too. In general, the modelled components include the main propulsion engines, gearboxes, shafts, and propellers. In some cases, auxiliary power generation is modelled too. Control strategy applications on the other hand require the use of dynamic models (Zahedi et al., 2014; Geertsma et al., 2018; Haseltalab et al., 2019). In the specific case of energy management applications, both steady state (Zhu et al., 2018) and dynamic (Al-Falahi et al., 2018; Kalikatzarakis et al., 2018; Haseltalab and Negenborn, 2019) models of the energy system can be used.

Prediction of fuel consumption in certain environmental and operational conditions usually follows two modelling strategies. The first combines steady state energy system models with semi-empirical resistance prediction models (Lu et al., 2015) or more advanced computer fluid dynamics models (Avgouleas and Sclavounos, 2014). The second uses statistical models to predict fuel consumption in a one step calculation as in Coraddu et al. (2017) or in a two step main shaft propulsion power and fuel consumption prediction (Farag and Ölçer, 2020). A review of statistical models and methods used in the fuel consumption prediction of ships can be found in Gkerekos et al. (2019), Huang et al. (2022). The modelling strategy in this paper differs from this practice as the main aim is to preserve the first principle understanding of the system components.

Finally, energy performance analysis and optimisation at a component and subsystem level is also dominated by the use of steady state models, although these models can vary in their level of detail. For example, applications in finding optimal configurations use look-up tables (Dedes et al., 2012, 2016; Ancona et al., 2018), but applications on optimising thermodynamic working cycles require much more detailed models based on energy efficiency analysis (Sakalis and Frangopoulos, 2018) or even exergy analysis (Baldi et al., 2015a,b; Shu et al., 2017). Those studies focus on the low-level examination of the system, nevertheless, they confirm the general practice of sacrificing time dependency for more detailed models and a higher number of simulations.

1.2. Gaps

Researchers use actual operational and environmental conditions coupled with empirical models to examine energy efficiency gains from optimising operational decisions such as weather routing, vessel speed selection, and optimal loading of the vessel. When the focus lies on alternative system configurations and settings, they tend to test their technological innovations on scenarios that are not representative of the actual conditions at sea. Hence, a methodology on the aggregate effect of actual operational and environmental conditions is missing. Moreover, ship energy systems consist of a large number of interacting components that show non-linear behaviour (Baldi, 2016). Modelling discrepancies of those components result in accumulating prediction errors. On the occasion that large datasets of operational data are available, calibration and validation of the whole energy system model become challenging too. At a component level, there is a number of examples of calibrating, validating, and enhancing the accuracy of different models as in the case of main diesel engines (Hountalas, 2000; Coraddu et al., 2018; Kalikatzarakis et al., 2021; Coraddu et al., 2021). However, such methodologies at a whole system level are lacking due to different sensor availability of monitoring platforms and diversity in system architecture.

1.3. Aim and contribution

The main aim of this paper is to develop an accurate and computationally low-cost operational data-driven methodology that can predict the fuel consumption and carbon intensity of ship operations under the aggregate effect of diverse and uncertain operational and environmental conditions. This methodology can be used to establish optimal settings and evaluate future design alternatives. Therefore, the contribution of this paper can be summarised as follows:

- It provides a methodology to build a digital twin of ship energy systems that can be used to evaluate operational decisions, design changes, and contribute to enhanced future designs.
- It proposes a novel methodology to account for realistic operational and environmental conditions.
- It proposes a systematic methodology to validate models of the whole energy system in the presence of large operational datasets.
- It proposes statistical modelling techniques to compensate for uncertainty related to sensor measurements and the limited availability of information from shipbuilders and component manufacturers.
- It provides a case study that demonstrates the capability of steady-state models coupled with data-driven techniques in accurately predicting fuel consumption over actual dynamic and quasi-static sailing conditions.
- It provides a direct comparison between electrical and mechanical propulsion over actual sailing profiles.

The rest of the paper is organised as follows. Section 2 presents the main characteristics of the examined vessel and the used datasets. Section 3 presents our proposed methodology to build and utilise a digital twin of the vessel's energy system. Section 4 provides a description of the data-driven techniques applied. Section 5 provides all accuracy metrics for the developed models. Section 6 presents our results and Section 7 the drawn conclusions. To assist the readability of the paper, Table 1 summarises the used acronyms and symbols.

2. Case study vessel and dataset description

The case study vessel in this paper is an Ocean-going Patrol Vessel (OPV) of The Royal Netherlands Navy (RNLN). A schematic representation of its energy system can be seen in Fig. 1. Two controllable pitch propellers are driven either mechanically by two main diesel engines rated at 5,400 kW, or electrically by two electrical motors rated at 400 kW. Propeller shaft speed is reduced by two gearboxes which utilise one speed reduction stage of 4.355 in the case of mechanical propulsion or two stages with a total reduction ratio of 17.880 in the case of electrical propulsion. Finally, electrical power is produced by three diesel generators rated at 920 kW. All component specifications can be found in Table 2. The proposed methodology utilises operational data logged by the automation system of the vessel. Cleaning and preprocessing was done as in Karagiannidis and Themelis (2021), but vessel speed was selected as the prime parameter and the top and bottom 0.1% percentile was used to discard outliers instead of standard deviation. The dataset is characterised by a sampling frequency of 3 s and covers a time window of 15 months. The main parameters used in this paper are reported in Table 3. These parameters are all measured by the automation system, except for the thrust parameter, which is

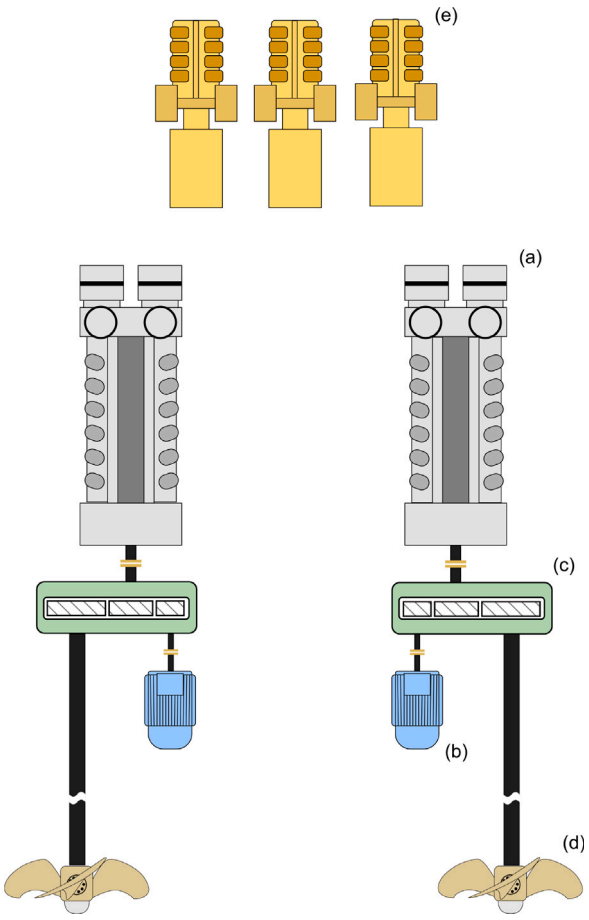

Fig. 1. The case study energy system: (a) main diesel engine, (b) electrical motor, (c) gearbox, (d) controllable-pitch propeller, (e) diesel generator.

Table 2
Component specifications.

Diesel generators	Value	Unit
Nominal power	910	[ekW]
Nominal speed	1800	[rpm]
Nominal fuel consumption (ISO)	235	[kg/h]
Main diesel engines		
Nominal power	5400	[kW]
Nominal speed	1000	[rpm]
Nominal fuel consumption (ISO)	1077	[kg/h]
Electrical motors		
Nominal power	400	[kW]
Nominal speed	1788	[rpm]
Gearboxes		
Reduction ratio (MDE)	4.355	[–]
Reduction ratio (M)	17.880	[–]
CPP Propellers		
Diameter	3.2	[m]
Nominal pitch to diameter	1.221	[–]
Zero-thurst pitch to diameter	0.144	[–]

estimated based on the dataset enrichment methodology described in the authors' earlier work (Vasilikis et al., 2022).

The examined vessel uses a number of operational modes in order to serve its multifunction mission. The focus of this study lies in the two main operational modes. The first one is designed for sailing on two main diesel engines while in transit, from now on referred to as Mechanical Mode (MM). The second main mode is designed for patrolling or low speed transits up to 10 knots on the two electric motors, from now on referred to as Electrical Mode (EM). Fig. 2 provides distributions of dataset parameters for the examined two propulsion options. Vessel operation below 5 knots is discarded as part of manoeuvring which does not have an important impact on attained energy performance and carbon footprint.

Table 3
Dataset parameters.

Parameter	Unit
Vessel speed through water	[knots]
Propeller pitch to diameter	[–]
Propeller thrust	[kN]
Propeller shaft speed	[rpm]
Propeller shaft torque	[kNm]
Electrical motors power	[kW]
Generated electrical power	[kW]
Main diesel engines fuel consumption	[kg/h]
Diesel generators fuel consumption	[kg/h]
Ambient air temperature	[°]
Time	[sec]

3. Methodology

The methodology of this paper proposes a two-phase approach to accurately predict the energy performance of complex ship energy systems under realistic operational and environmental conditions, by leveraging steady-state first-principle models (Coraddu et al., 2014; Sui et al., 2019; Vasilikis et al., 2022) and the high-frequency operational data described in Section 2, as follows:

- **Phase I**: a digital twin (DT) (Grieves and Vickers, 2017; Mauro and Kana, 2023) of the vessel's hybrid energy system is developed to capture the quasi-static behaviour of the vessel in terms of energy, fuel consumption, and emissions. Due to the hybrid approach of using data-driven and first-principle techniques, we can achieve accurate predictions that capture the aggregate effect of operational and environmental uncertainty. The description of this DT is reported in Section 3.1 and its validation in Section 5.
- **Phase II**: the developed DT is employed in predicting the energy performance (i.e., fuel consumption) and carbon intensity of the vessel over a number of actual voyages, and it also provides a direct comparison between Mechanical Mode (MM) and Electrical Mode (EM).

A schematic representation of the methodology can be found in Fig. 3.

3.1. Phase I: Digital twin development

The developed DT predicts the fuel consumption of main diesel engines and generators and the propeller shaft torque for tuples of different vessel speed, propeller thrust, and ambient temperature. For each component depicted in Fig. 4, a short description of the modelling approach follows in the next subsections.

First, the model evaluates water speed in the ship's wake v_a from vessel speed v:

$$v_a = (1 - w)\, v\,, \tag{1}$$

using Taylor's wake fraction w which is provided by towing tank tests in Fig. 5. Next, it evaluates rotational speed n and pitch p of the controllable-pitch propeller based on an iteration algorithm described in Fig. 6. This algorithm iterates to the pitch setting for the given vessel speed using the fixed-pitch propeller matching algorithm and the ship's combinator curve as reported in Stapersma and Klein Woud (2005) to estimate rotational speed. Propeller's thrust coefficient $K_{T,ship}$ curve is provided by:

$$K_{T,ship} = \frac{T}{\rho\, v_a^2\, D^2}\, J^2\,, \tag{2}$$

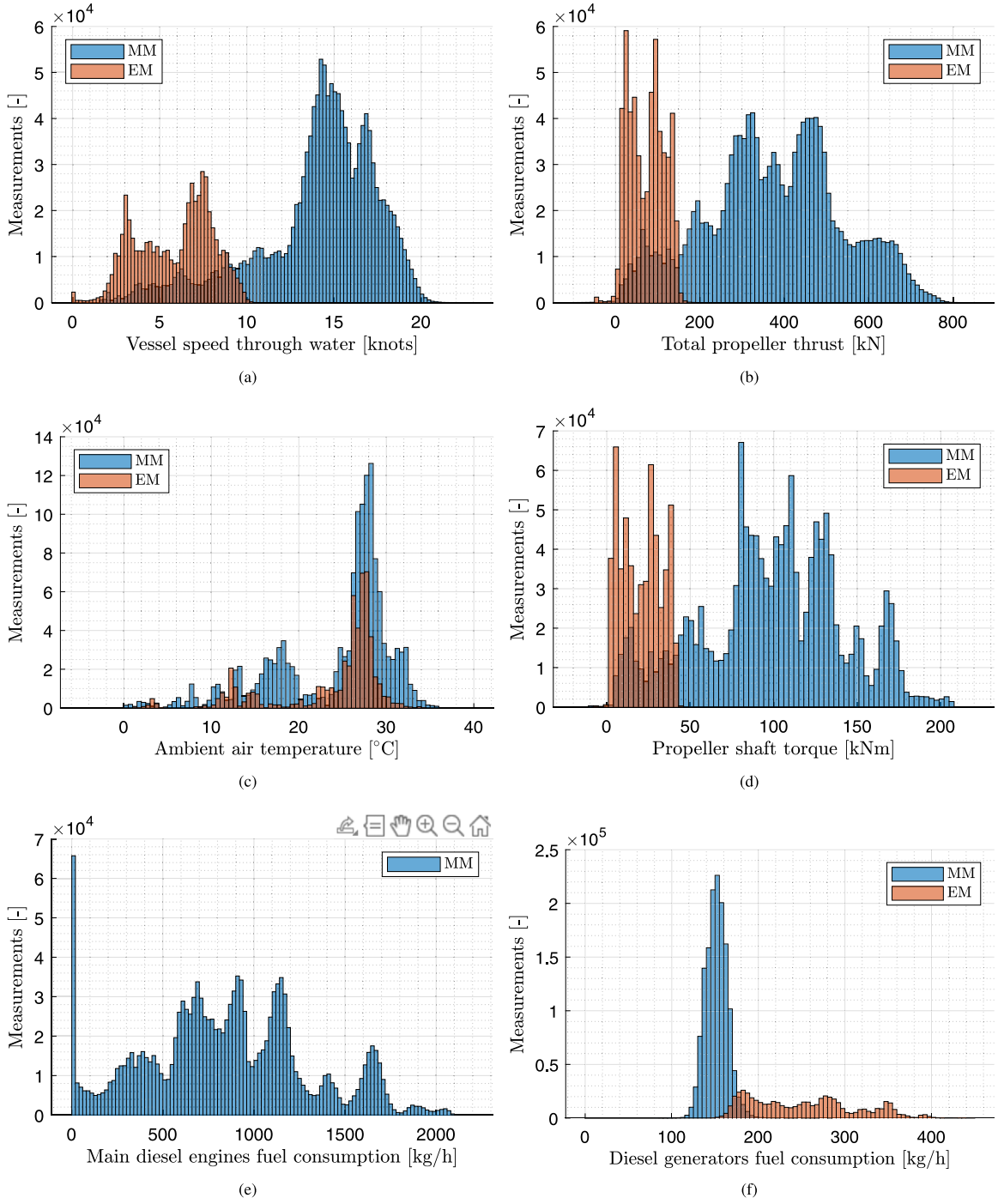

Fig. 2. Dataset parameters distribution.

where T is propeller thrust, ρ is water density, D is propeller diameter and J is the advance coefficient. The initial value for virtual shaft speed $n_{\text{virt,i}}$ is assumed a linear function of vessel speed:

$$n_{\text{virt,i}} = c_1\, v - c_0, \qquad v > 2\text{knots}\,. \tag{3}$$

Propeller pitch is provided as a function of virtual shaft speed n_{virt} using the corresponding combinator curve for the selected operational mode in Fig. 7. Thrust coefficient curves K_{T} are established with the propeller open water diagrams, as shown in Fig. 8. Propeller speed is evaluated using the advance coefficient as follows:

$$n = \frac{v_{\text{a}}}{J\, D}\,. \tag{4}$$

Virtual shaft speed n_{virt} is provided by:

$$n_{\text{virt}} = \frac{p - p_0}{p_{nom} - p_0}\, n\,, \tag{5}$$

where p_0 is zero thrust pitch and p_{nom} is nominal pitch. Following the successful convergence of the iteration procedure, the pitch value and the advance coefficient are used in to establish the torque coefficient in

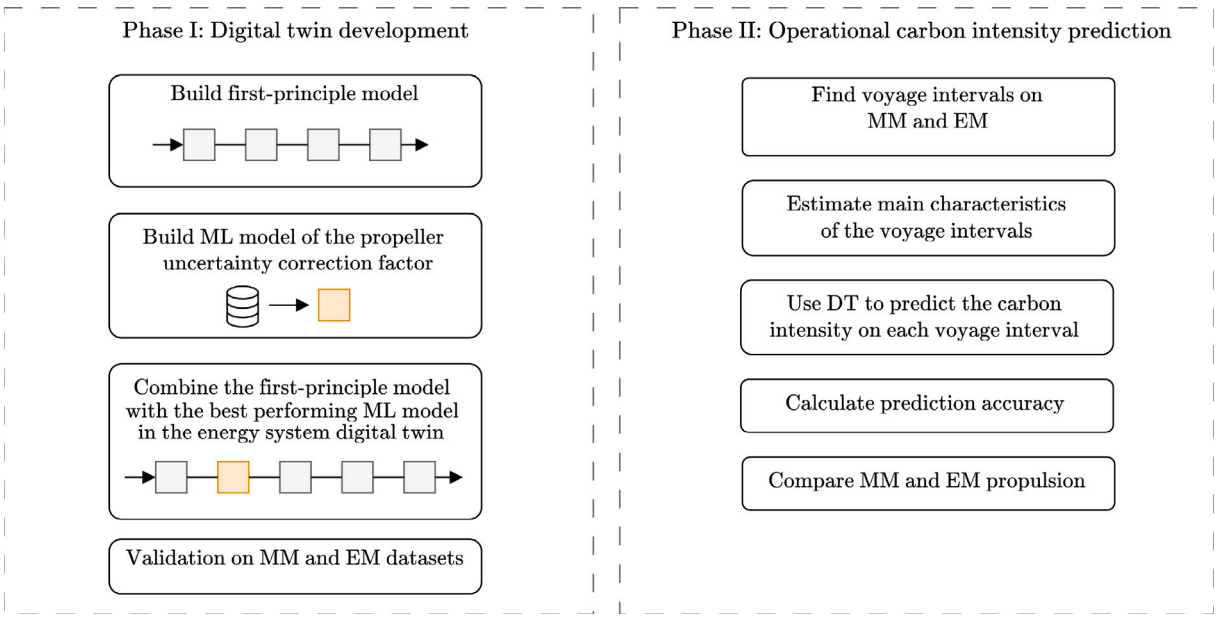

Fig. 3. Schematic representation of the proposed methodology.

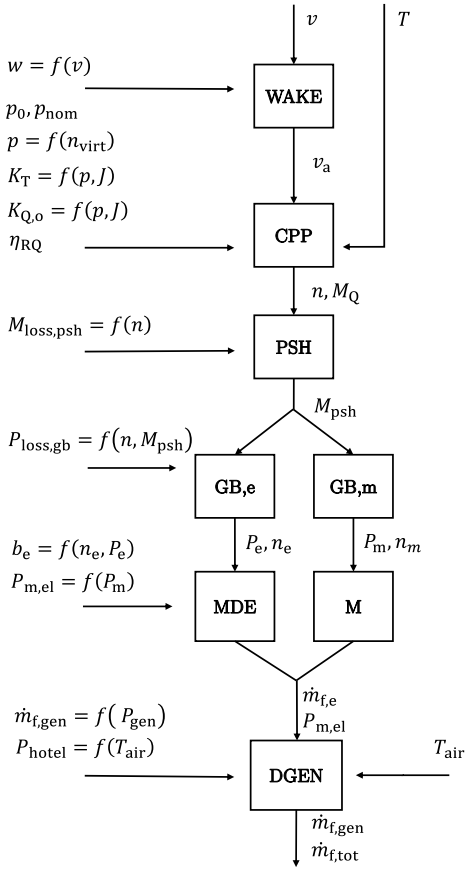

Fig. 4. Flowchart of the Digital Twin.

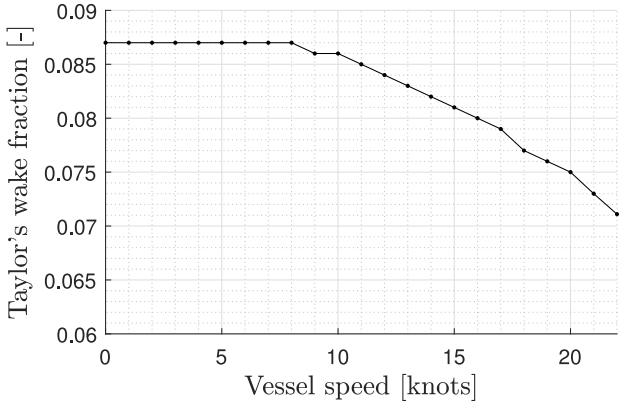

Fig. 5. Taylor's wake fraction based on towing tank tests.

open water conditions $K_{Q,o}$ using Fig. 9. Propeller torque in open water conditions $M_{Q,o}$ is then estimated from:

$$M_{Q,o} = K_{Q,o}\,\rho\,n^2\,D^5\,, \tag{6}$$

while propeller torque M_Q is evaluated using the relative rotative efficiency η_{RQ}:

$$M_Q = \frac{M_{Q,o}}{\eta_{RQ}}\,, \tag{7}$$

the background of which is discussed in the following two paragraphs.

The use of propeller open water diagrams in predicting propeller thrust, torque, and speed is based on decoupling the problem of the self-propelled ship into the problem of open water propeller operation and the problem of the towed ship (Taylor, 1910). Typically, a selection between thrust or torque identity is made by introducing relative rotative efficiency. It is usual to select the first option of thrust identity, suggesting that the thrust coefficient stays the same in actual and open water conditions (ITTC, 2014). Literature provides semi-empirical formulas for evaluating relative rotative efficiency as in Holtrop (1984). The use of those formulas corresponds to nominal design conditions, and their accuracy on modern ships and off-design conditions has not been examined (Carlton, 2019). Only recently, was the effect of control strategies and scaling discussed further Huijgens et al. (2022).

Nonetheless, the availability of operational data offers the opportunity to assess the accuracy of those formulas in design and off-design conditions. The utilised IPMS dataset includes measurements of propeller torque, pitch, rotational speed, and vessel speed. Eq. (6) provides

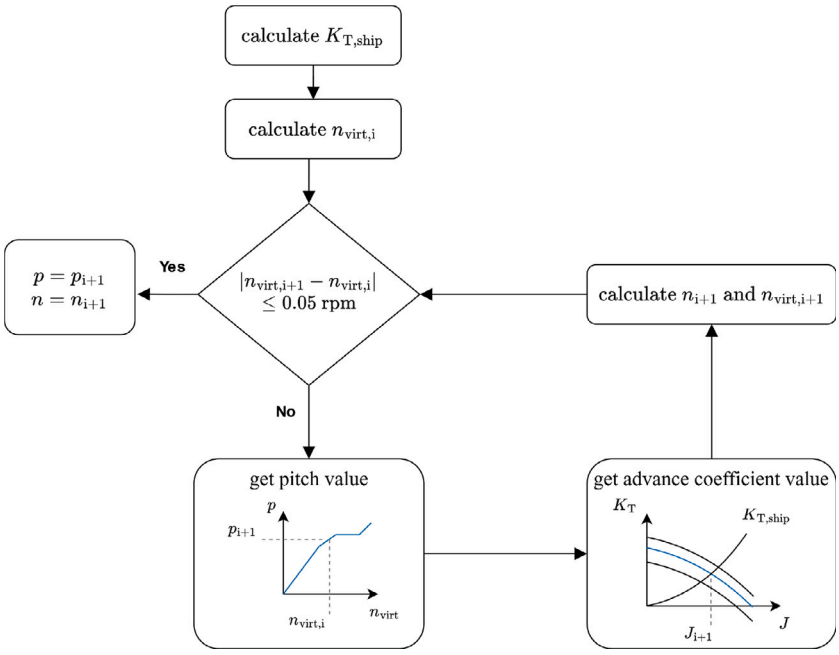

Fig. 6. Controllable pitch propeller pitch and rotational speed evaluation algorithm.

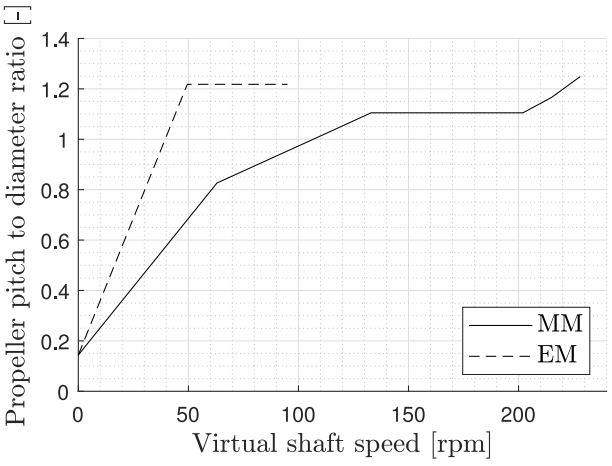

Fig. 7. Combinator curves.

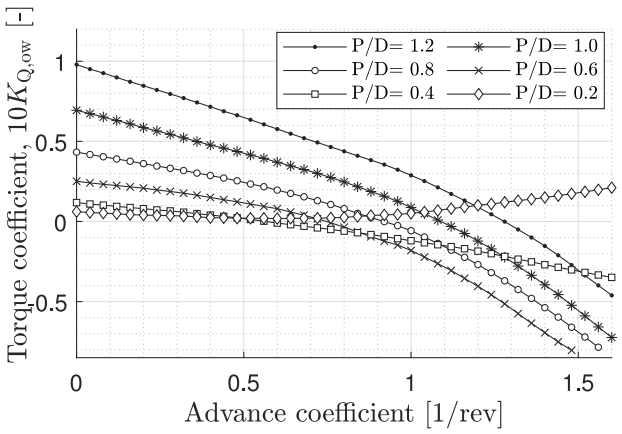

Fig. 9. Torque coefficient open water diagram.

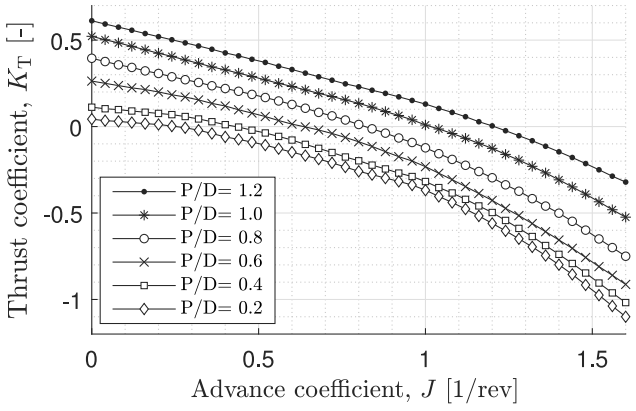

Fig. 8. Thrust coefficient open water diagram.

an estimation of propeller torque in open water conditions. In theory, the fraction of this torque value with measured torque provides an estimation of the relative rotative efficiency $\hat{\eta}_{RQ}$:

$$\hat{\eta}_{RQ} = \frac{M_{Q,o}}{M_Q}, \tag{8}$$

where the hat symbol is used to distinguish our estimation to the theoretical value η_{RQ}, as it involves uncertainty related to the accuracy of our measurements and of the diagrams used. Parameters like the thrust deduction factor t, wake factor w, and the relative rotative efficiency are usually used to compensate for this uncertainty (MAN Energy Solutions, 2018). In this paper, the estimated relative rotative efficiency based on Eq. (8), from this point called propeller uncertainty correction factor, is modelled as a statistical model following the procedure described on Section 4.

Furthermore, the model evaluates propeller shaft torque M_{psh} using the propeller torque and propeller shaft torque losses $M_{loss,psh}$ according to:

$$M_{psh} = M_Q + M_{loss,psh}, \tag{9}$$

Table 4
Original brake specific fuel consumption contour lines provided by the manufacturer and percentage correction.

b_e [g/kWh]	Correction	b_e [g/kWh]	Correction	b_e [g/kWh]	Correction
236	−1.7%	213	no	199	+1.5%
230	−1.7%	209	no	195	+1.5%
217	no	204	no	193	+2.1%

where the latter is provided as a linear function of shaft speed by the manufacturer,

$$M_{\text{loss,psh}} = c_3\, n + c_2\,, \tag{10}$$

Consequently, propeller shaft power is evaluated from $P_{\text{psh}} = M_{\text{psh}}\, n\, 2\pi$. Main diesel engine power P_e and electrical motor power P_m are estimated based on gearbox losses $P_{\text{loss,gb}}$:

$$P_e = P_{\text{psh}} + P_{\text{loss,gb}}\,, \tag{11}$$

$$P_m = P_{\text{psh}} + P_{\text{loss,gb}}. \tag{12}$$

The linear torque losses model proposed in Godjevac et al. (2015) is used. It is calibrated with the data provided by the gearbox manufacturer as a function of input power and speed:

$$P_{\text{loss,gb}} = \begin{cases} c_6\, P_e + c_5\, {n_e}^2 + c_4\, n_e & \text{(MM)}, \\ c_9\, P_m + c_8\, {n_m}^2 + c_7\, n_m & \text{(EM)}, \end{cases} \tag{13}$$

where n_e and n_m derive using the corresponding speed reduction ratios r_e and r_m:

$$n_e = r_e\, n\,, \tag{14}$$

$$n_m = r_m\, n. \tag{15}$$

Following the substitution of Eqs. (11) and (12), gearbox losses are given from:

$$P_{\text{loss,gb}} = \frac{c_6\, P_{\text{psh}} + c_5\, {n_e}^2 + c_4\, n_e}{(1 - c_6)}\,, \tag{16}$$

$$P_{\text{loss,gb}} = \frac{c_9\, P_{\text{psh}} + c_8\, {n_m}^2 + c_7\, n_m}{(1 - c_9)}. \tag{17}$$

Fuel consumption of the main diesel engines $\dot{m}_{f,e}$ is evaluated from the specific fuel consumption b_e as:

$$\dot{m}_{f,e} = \frac{b_e\, P_e\, 3600}{1000}\,, \tag{18}$$

which is interpolated using speed n_e and power P_e from Fig. 10. This look-up table was built out of the brake specific fuel consumption contour curves provided by the manufacturer in van Straten and de Boer (2012), corrected with the available dataset according to Table 4.

The electrical power delivered to the motors $P_{\text{m,el}}$ is evaluated based on their energy efficiency η_m and delivered power P_m:

$$P_{\text{m,el}} = \frac{P_m}{\eta_m}. \tag{19}$$

The energy efficiency of the motors is modelled as a function of the delivered power as described hereafter:

$$\eta_m = c_{12}\, z^2 + c_{11}\, z + c_{10}\,, \tag{20}$$

where

$$z = \log P_m. \tag{21}$$

The constants are estimated based on the test results for an induction motor provided in Kalikatzarakis et al. (2018) (see Fig. 11).

Fuel consumption of the diesel generators $\dot{m}_{f,\text{gen}}$ is derived from the specific fuel consumption b_{gen} as:

$$\dot{m}_{f,\text{gen}} = \frac{b_{\text{gen}}\, P_{\text{gen}}\, 3600}{1000}. \tag{22}$$

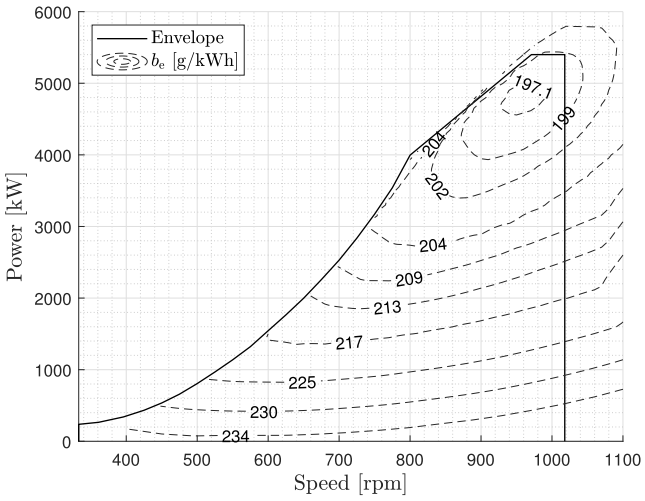

Fig. 10. Brake specific fuel consumption map of the main diesel engines.

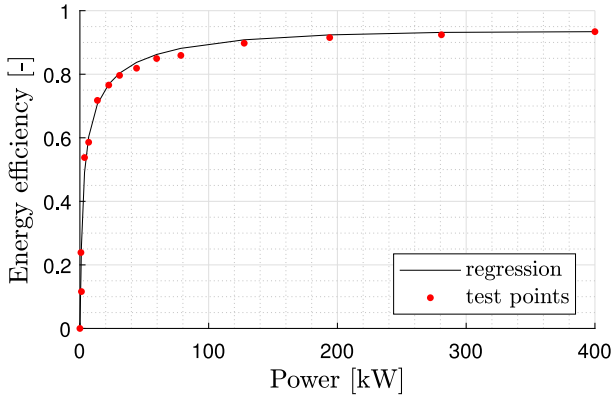

Fig. 11. Electrical motor's energy efficiency against produced power.

Specific fuel consumption is modelled using the available dataset parameters as a function of the total generated electrical power P_{gen} (see Fig. 12):

$$b_{\text{gen}} = \frac{c_{14}}{P_{\text{gen}}} + c_{13}\,, \tag{23}$$

which is the sum of the hotel load P_{hotel} and the power provided to the electrical motors $P_{\text{m,el}}$:

$$P_{\text{gen}} = P_{\text{hotel}} + P_{\text{m,el}}. \tag{24}$$

The system and auxiliary electrical load is influenced by many factors, such as the mission of the vessel that determines which sensor and weapon systems are active and the activities undertaken by the crew. From the analysis of our dataset, we have established that the correlation with outside air temperature T_{air} is the strongest correlation of all parameters. This is caused by the fact that the electrical capacity of the chilled water plant for cooling of all systems is one of the largest electrical non-propulsion loads that is directly influenced by the outside air temperature. Thus, hotel electrical load P_{hotel} is modelled as a quadratic function of the external air temperature T_{air} (see Fig. 13):

$$P_{\text{hotel}} = c_{17}\, {T_{\text{air}}}^2 + c_{16}\, T_{\text{air}} + c_{15}. \tag{25}$$

Ultimately, total fuel consumption of the vessel $\dot{m}_{f,\text{tot}}$ is provided by:

$$\dot{m}_{f,\text{tot}} = \dot{m}_{f,e} + \dot{m}_{f,\text{gen}}. \tag{26}$$

All model constants of the developed digital twin can be found in Table 5.

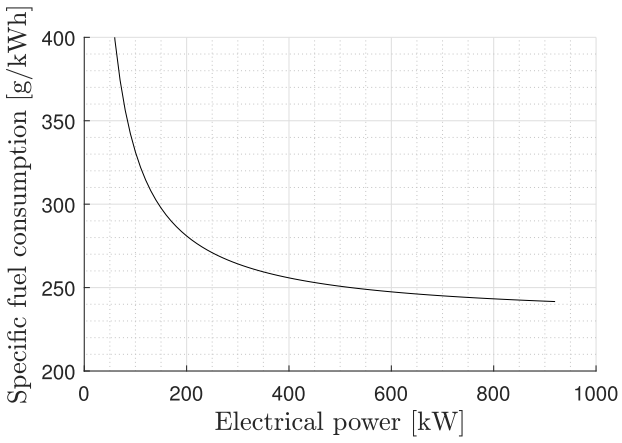

Fig. 12. Diesel generators' specific fuel consumption against produced electrical power.

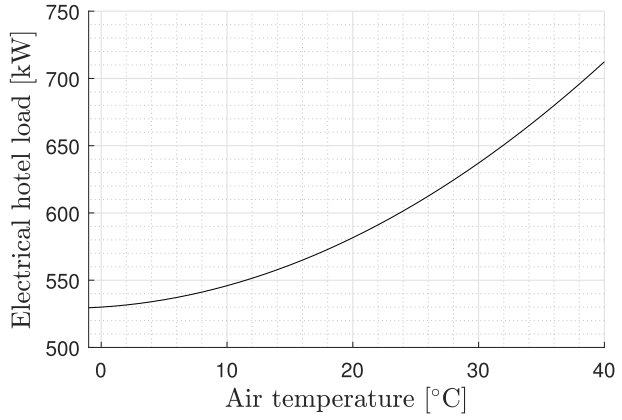

Fig. 13. Electrical hotel load as a function of ambient air temperature.

Table 5
Model Constants.

Constant	Value	Constant	Value	Constant	Value
Initial virtual shaft speed		Gearbox losses (EM)		Diesel generators	
c_0	11	c_7	0.00297	c_{13}	230.7
c_1	7.9	c_8	1.025e−05	c_{14}	10.05
		c_9	0.0050		
Propeller shaft losses		Electrical Motors		Ambient Temperature	
c_2	1.4	c_{10}	0.2161	c_{15}	530
c_3	0.0134	c_{11}	0.553	c_{16}	0.6
		c_{12}	−0.1065	c_{17}	0.099
Gearbox Losses (MM)					
c_4	0.0081				
c_5	9.002e−05				
c_6	0.0050				

3.2. Phase II: Carbon intensity evaluation

The second phase of our methodology examines the hypothesis that the developed DT can accurately predict carbon emissions over a selection of actual voyage intervals in line with existing regulations (MEPC, 2021b). The selection of those intervals involved finding periods of at least four hours of continuous sailing on the same operational mode. The total duration Δt, covered distance Δs, and total amount of consumed fuel $M_{\mathrm{f,tot}}$ was approximated by midpoint rule numerical integration as follows:

$$\Delta t \;=\; \int dt \;\simeq\; \sum_{j=1}^{N} \delta t \;=\; N\;\delta t\,, \tag{27}$$

$$\Delta s \;=\; \int v_{\log}\; dt \;\simeq\; \sum_{j=1}^{N} v_{\log}\;\delta t\,, \tag{28}$$

$$M_{\mathrm{f,tot}} \;=\; \int \dot{m}_{\mathrm{f,tot}}\; dt \;\simeq\; \sum_{j=1}^{N} \dot{m}_{\mathrm{f,tot}}\;\delta t. \tag{29}$$

Mean sea margin $\overline{\mathrm{SM}}$ was evaluated as the mean difference of thrust and calm water resistance R_0:

$$\overline{\mathrm{SM}} \;=\; \overline{\left(T - R_0\right)/R_0}. \tag{30}$$

Mean speed $\overline{v} = \Delta s/\Delta t$ and Carbon Intensity (CI) derive as:

$$\mathrm{CI} \;=\; \frac{M_{\mathrm{f,tot}}\; f_{\mathrm{CO2}}}{\Delta s}\,, \tag{31}$$

where f_{CO2} is the carbon factor equal to 3.206 for diesel oil according to EEDI regulations (MEPC, 2014). The evaluated characteristics of the selected intervals can be found in Tables 10 and 11 in the case of mechanical and electrical propulsion, respectively. The prediction accuracy of the selected intervals is examined using the Mean Average Percentual Error (MAPE) of total fuel consumption $\dot{m}_{\mathrm{f,tot}}$, and the Absolute Percentage Error (APE) of the predicted amount of consumed fuel $M_{\mathrm{f,tot}}$, consequently carbon intensity.

The last step of phase II is the selection of non-dynamic intervals to simulate the energy performance of the vessel in MM and EM and provide a direct comparison between them.

4. Data-driven models

One of the objectives of this study is to develop a model for predicting the propeller uncertainty correction factor, denoted as $\hat{\eta}_{\mathrm{RQ}}$, based on the input parameters outlined in Table 6. This model will utilise the data described in Section 2. Fig. 14 illustrates the histogram of relative frequencies for the target feature in both MM and EM. This learning problem can be formulated as a supervised Machine Learning (ML) problem, specifically a regression problem (Shalev-Shwartz and Ben-David, 2014). In regression analysis, an input space $\mathcal{X} \subseteq \mathbb{R}^d$ is comprised of d features (in this case, the four parameters in Table 6). The output space, $\mathcal{Y} \subseteq \mathbb{R}$, corresponds to $\hat{\eta}_{\mathrm{RQ}}$. A dataset of n examples, denoted as $\mathcal{D}_n = (\boldsymbol{x}_1, y_1), \ldots, (\boldsymbol{x}_n, y_n)$, represents input/output relationships where $\boldsymbol{x}_i \in \mathcal{X}$ and $y_i \in \mathcal{Y}\ \forall i \in 1, \ldots, n$. The aim is to learn the unknown input/output function $\mu : \mathcal{X} \to \mathcal{Y}$ based solely on $\mathcal{D}n$. An ML regression algorithm $\mathscr{A}$, characterised by its hyperparameters $\mathcal{H}$, selects a model f from a set of potential models $\mathcal{F}$ based on available data $\mathscr{A}\mathcal{H} : \mathcal{D}_n \times \mathcal{F} \to f$. The set $\mathcal{F}$ is typically unknown and depends on the choices of $\mathscr{A}$ and $\mathcal{H}$. Various ML algorithms exist in the literature (Shalev-Shwartz and Ben-David, 2014; Goodfellow et al., 2016; Fernández-Delgado et al., 2014; Wainberg et al., 2016). However, according to the no-free-lunch theorem (Wolpert, 2002), there is no a priori method for determining the best ML algorithm for a specific application. Therefore, this study will consider an assortment of state-of-the-art ML algorithms.

The accuracy of model f in approximating μ is evaluated using a prescribed metric $M : f \to \mathbb{R}$. Multiple metrics are available for regression analysis in ML (Aggarwal, 2015). However, due to the physical significance of $\hat{\eta}_{\mathrm{RQ}}$, this study will focus on four primary metrics: Mean Absolute Error (MAE), Mean Absolute Percentage Error (MAPE), Relative Error in Percentage (REP), and the Coefficient of Determination (R^2). To identify the most suitable ML algorithms and their corresponding optimal hyperparameters, as well as to evaluate the performance of the final model based on the desired metrics, a statistically consistent Model Selection (MS) and Error Estimation (EE) process was conducted. The methodology for this process is detailed in Section 4.2, following the recommendations presented in Oneto (2020).

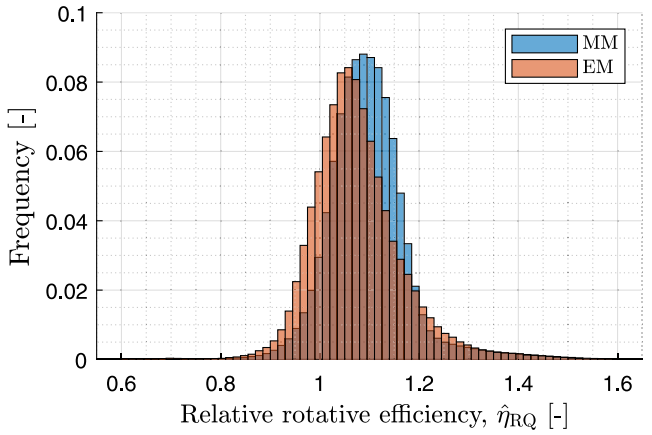

Fig. 14. Distribution of propeller uncertainty correction factor (relative rotative efficiency obtained from the IPMS dataset), $\hat{\eta}_{RQ}$.

Table 6
List of inputs and outputs of the ML models.

Space	Symbol	Description	Unit
Input	v	Vessel speed	[kn]
	T	Thrust	[kN]
	p	Pitch	[–]
	n	Shaft speed	[rpm]
Output	$\hat{\eta}_{RQ}$	Propeller uncertainty correction factor	[–]

4.1. Machine learning models

This section provides a concise overview of the four algorithms employed in this study, highlighting the fundamental concepts, usage, and hyperparameters associated with each algorithm. The chosen algorithms represent the most effective approaches within the four primary families of ML regression algorithms (Shalev-Shwartz and Ben-David, 2014; Goodfellow et al., 2016; Fernández-Delgado et al., 2014; Wainberg et al., 2016): Linear Methods (Zou and Hastie, 2005), Kernel Methods (Shawe-Taylor and Cristianini, 2004), Ensemble Methods (Zhou, 2012), and Neural Networks (Goodfellow et al., 2016).

4.1.1. Linear methods

Regularised Least Squares (RLS) is a regression method that introduces a regularisation term to the traditional least squares problem to control the complexity of the model and prevent overfitting. The objective of RLS is to minimise the sum of squared residuals, similar to ordinary least squares, but with an additional penalty term that discourages large values of the model parameters. The regularisation term is typically a function of the model parameters, such as the L2 norm (also known as Ridge regression) or the L1 norm (also known as Lasso regression). The L2 norm encourages small parameter values, leading to a more stable model with lower variance, while the L1 norm can lead to sparse solutions, where some parameters are exactly zero, effectively performing feature selection. The balance between the fit to the data and the regularisation is controlled by the only hyperparameter of this algorithm λ. A larger λ increases the impact of the regularisation term, leading to a simpler model, while a smaller λ allows the model to fit more closely to the data, potentially at the risk of overfitting.

4.1.2. Neural networks

Neural Networks, inspired by human brain neurons, are complex networks built from numerous perceptrons (Rosenblatt, 1958). Their structure consists of layers linked by weights, determined through backpropagation (Rumelhart et al., 1986). A network with a single hidden layer is a shallow neural network, while one with multiple hidden layers is a deep neural network. Deep networks excel in complex computations and learning high-level features, improving predictive accuracy. Despite Cybenko's Universal Approximation Theorem (Cybenko, 1989) suggesting equal representational capacities for both architectures, deep networks often outperform shallow ones in tasks like natural language processing and image analysis.

Given our study's limited sample size and unstructured features, we chose a shallow neural network to avoid overfitting (Bishop, 1995; Goodfellow et al., 2016). We used the Multilayer Perceptron Network (MLP) (Bishop, 1995; Goodfellow et al., 2016) with Dropout architecture, which has a single hidden layer. The training process uses adaptive subgradient methods for dynamic learning rate adjustments. We optimised various hyperparameters during the MS phase (Goodfellow et al., 2016), including the number of neurons in the hidden layer, dropout rate, batch size percentage, learning rate, fraction of gradient to retain, learning rate decay, and the activation function. By tuning these hyperparameters, we optimised the performance of our MLP model for the given task.

4.1.3. Kernel methods

Kernel Methods are algorithms that use the 'Kernel trick' to transform linear methods for non-linear problems (Scholkopf, 2001). They use kernel functions to map input data into a higher-dimensional space, enabling linear separability for non-linear problems. This mapping allows the computation of inner products in the feature space without explicit high-dimensional computations, extending linear algorithms to work efficiently in the transformed space. Kernel methods balance empirical performance and model complexity (Shawe-Taylor and Cristianini, 2004; Shalev-Shwartz and Ben-David, 2014). Empirical performance, measured by a pre-defined metric, assesses the model's fit and prediction reliability. Model complexity, evaluated by various measures, assesses the solution space complexity. Higher complexity can fit more functions but risks overfitting. Therefore, kernel methods aim to strike an optimal balance between these two aspects: achieving high performance on the data without over-complicating the model.

Support Vector Regression (SVR) is a well-known and efficient Kernel method technique. It uses Support Vector Machines (SVMs) principles and hyperparameters like the kernel function, often set to a Gaussian or Radial Basis Function (RBF) kernel for its flexibility in modelling complex, non-linear relationships (Keerthi and Lin, 2003). The kernel hyperparameter, γ, controls the non-linearity of the decision boundary and the kernel function's shape and scale. A small γ leads to a more linear boundary, while a large γ creates a more complex, non-linear boundary. The regularisation hyperparameter, C, balances model accuracy and solution complexity. A small C allows more misclassifications for a simpler boundary, while a large C aims for higher accuracy, potentially at the cost of a more complex boundary. Both γ and C are critical to the performance of the SVR model and need to be meticulously tuned during the MS phase to ensure optimal model performance.

4.1.4. Ensemble methods

Ensemble methods, like Random Forests (RF), use the 'wisdom of the crowd' principle by integrating many simple, independent models to form a more complex and effective one. RF are notable examples, using Decision Trees as their base models. A Decision Tree is a flowchart-like structure where each internal node represents a feature test, each branch shows the test's outcome, and each leaf node indicates the tree's output. A path from the root to a leaf represents a model rule. Decision Trees are built recursively to a specified depth, with each node constructed from the attribute and cut that best split the samples into two subsets, based on information gain. RF enhances bagging, a process where each tree is independently constructed using a bootstrap sample of the dataset, with random subset feature selection. This approach uses different bootstrap samples of the data for each tree and alters

how trees are constructed. RF splits each node using the best among a subset of predictors, randomly chosen at that node. The final prediction is derived from a straightforward majority vote. The accuracy of the final RF model primarily hinges on three factors: the number of trees in the forest, the accuracy of each tree, and the correlation between them. As the number of trees in the forest increases, the accuracy for RF converges to a limit. Simultaneously, it improves as the accuracy of each tree increases, and the correlation between them diminishes. Several hyperparameters shape the performance of the final model, including the number of trees, the number of samples to extract during the bootstrap procedure, the depth of each tree, the number of predictors used in each subset during the growth of each tree, and finally, the weights assigned to each tree.

4.2. Model selection and error estimation

MS and Empirical EE are critical tasks in the application of ML algorithms, focusing on hyperparameter tuning and performance evaluation. Resampling techniques, frequently used due to their effectiveness in various scenarios, will be implemented in this study. Though alternative methods exist within Statistical Learning Theory, they often underperform resampling techniques in practice. Resampling techniques work by resampling the original dataset $\mathcal{D}_n$ once or multiple times (n_r), either with or without replacement, to generate three independent datasets: the learning set $\mathcal{L}_l^r$, validation set $\mathcal{V}_v^r$, and test set $\mathcal{T}_t^r$, where $r \in 1, \dots, n_r$. These datasets adhere to the following conditions:

$$\mathcal{L}_l^r \cap \mathcal{V}_v^r = \emptyset, \qquad \mathcal{L}_l^r \cap \mathcal{T}_t^r = \emptyset, \tag{32}$$

$$\mathcal{V}_v^r \cap \mathcal{T}_t^r = \emptyset \qquad \mathcal{L}_l^r \cup \mathcal{V}_v^r \cup \mathcal{T}_t^r = \mathcal{D}_n \tag{33}$$

To perform MS, i.e., select the optimal combination of hyperparameters $\mathcal{H}$ from a set of possibilities $\mathfrak{H}$ for the algorithm $\mathscr{A}_\mathcal{H}$, we use the following procedure

$$\mathcal{H}^* : \quad \arg\min_{\mathcal{H}\in\mathfrak{H}} \sum_{r=1}^{n_r} M(\mathscr{A}_\mathcal{H}(\mathcal{L}_l^r), \mathcal{V}_v^r), \tag{34}$$

Here, $\mathscr{A}_\mathcal{H}(\mathcal{L}_l^r)$ represents a model built using algorithm $\mathscr{A}$ with its set of hyperparameters $\mathcal{H}$ and data $\mathcal{L}_l^r$, and $M(f, \mathcal{V}_v^r)$ is the desired metric. $\mathcal{H}^*$ should minimise error on a dataset independent from the training set since $\mathcal{L}_l^r$ is independent from $\mathcal{V}_v^r$.

To perform EE, which assesses the performance of the optimal model $f^{\mathscr{A}} = \mathscr{A}_\mathcal{H}(\mathcal{D}_n)$, we use the following procedure

$$M(f_{\mathscr{A}}^*) = \frac{1}{n_r} \sum_{r=1}^{n_r} M(\mathscr{A}_\mathcal{H}^*(\mathcal{L}_l^r \cup \mathcal{V}_v^r), \mathcal{T}_t^r). \tag{35}$$

Since the data in $\mathcal{L}_l^r \cup \mathcal{V}_v^r$ are independent of the ones in $\mathcal{T}_t^r$, $M(f_{\mathscr{A}}^*)$ is an unbiased estimator of the true performance, measured with the metric M, of the final model (Oneto, 2020).

In this work, we will rely on Complete 10-fold cross-validation, which means setting

$$n_r \leq \binom{n}{k}\binom{n-\frac{n}{k}}{k}, \tag{36}$$

$$l = (k-2)\frac{n}{k}, \tag{37}$$

$$v = \frac{n}{k}, \tag{38}$$

and

$$t = \frac{n}{k} \tag{39}$$

and the resampling must be done without replacement (Oneto, 2020). The large size of the two utilised datasets, 1,331,972 and 338,918 elements in MM and EM respectively, guarantee sufficient representation of all parameters in the learning, validation and testing datasets. Finally, the performance of the models in terms of accuracy is measured in accordance with different metrics: four quantitative (MAE, MAPE, REP, and R^2) (Naser and Alavi, 2021) and two qualitative such as the scatter plot actual versus predicted value and the histogram of the Absolute Percentage Error (Sainani, 2016).

Table 7
ML models validation: quantitative metrics (MAPE, MAE, REP) employed to evaluate performance of all examined algorithms (RF, SVR, MLP and RLS), on both propulsive modes (MM and EM).

Mechanical mode (MM)			
Algorithm	MAPE [%]	MAE [-]	REP [%]
RF	3.72 ± 0.04	0.041 ± 0.001	6.04 ± 0.02
SVR	3.97 ± 0.08	0.044 ± 0.001	6.41 ± 0.17
MLP	4.12 ± 0.05	0.045 ± 0.001	6.60 ± 0.10
RLS	6.71 ± 0.87	0.097 ± 0.013	9.75 ± 0.96
Electrical Mode (EM)			
RF	3.95 ± 0.01	0.043 ± 0.001	6.61 ± 0.03
SVR	4.94 ± 0.14	0.054 ± 0.002	7.86 ± 0.31
MLP	5.64 ± 0.04	0.061 ± 0.001	8.08 ± 0.06
RLS	9.78 ± 0.96	0.120 ± 0.002	12.61 ± 1.03

5. Models validation

This section provides the attained accuracy results of the four different ML algorithms of Section 4 used to model the propeller uncertainty correction factor, and the prediction accuracy of the developed digital twin described in Section 3.1.

5.1. Propeller uncertainty correction factor

In this section, we will report the performance of the ML models described in Section 4, using the validation approaches described in Section 4.2, and considering the different propulsive modes (i.e., MM and EM). In particular, we will compare the results of the different algorithms employed to build the models (RF, SVR, MLP, RLS).

Table 7 reports the different metrics used to evaluate the performance for all algorithms employed and the different propulsive modes. Fig. 15 provides a corresponding visual representation. Figs. 16 and 18 report the scatter plot for the best algorithm (RF) on each propulsive mode, while Figs. 17 and 19 report the absolute percentage error histogram of relative frequencies.

From Table 7 and Fig. 15, it is possible to observe that: (i) the selected RF algorithm outperformed the rest of the examined algorithms on both propulsion modes, (ii) the difference among the different algorithms was relatively bigger in EM compared to MM, with a 5.8% and 3.0% MAPE improvement, respectively. As expected, the RLS algorithm showed limited learning capability both on MM and EM. The inferior performance of the algorithms on EM compared to MM is possibly attributed to the pitch feature that stays almost constant on EM.

5.2. Digital twin

The prediction accuracy of the developed DT over the two operational mode datasets is reported here using the metrics in Section 4.2. Table 8 shows the DT performances using the most performing ML model (RF), assessed over the IPMS operational data on both MM and EM. The prediction capability of the DT accounting for the effect of actual operational and environmental conditions is confirmed by total fuel consumption MAPE of 3.7% in EM and 4.9% in MM. MAE values of main diesel engines and diesel generators also stand below 2% of nominal values. The prediction accuracy of the other parameters lies below 5.5% MAPE as well. Considering that both datasets contain highly dynamic operating points and that the logging rate of 3 s did not average this behaviour, the prediction capability of the quasi-static approach used for the DT is confirmed.

Table 9 shows the DT performances without using an ML model. Relative rotative efficiency was estimated using the semi-empirical formula for twin-screw ships provided by Holtrop and Mennen (1982). This formula uses hull prismatic coefficient, longitudinal centre of buoyancy, and nominal propeller pitch to diameter ratio, resulting in a

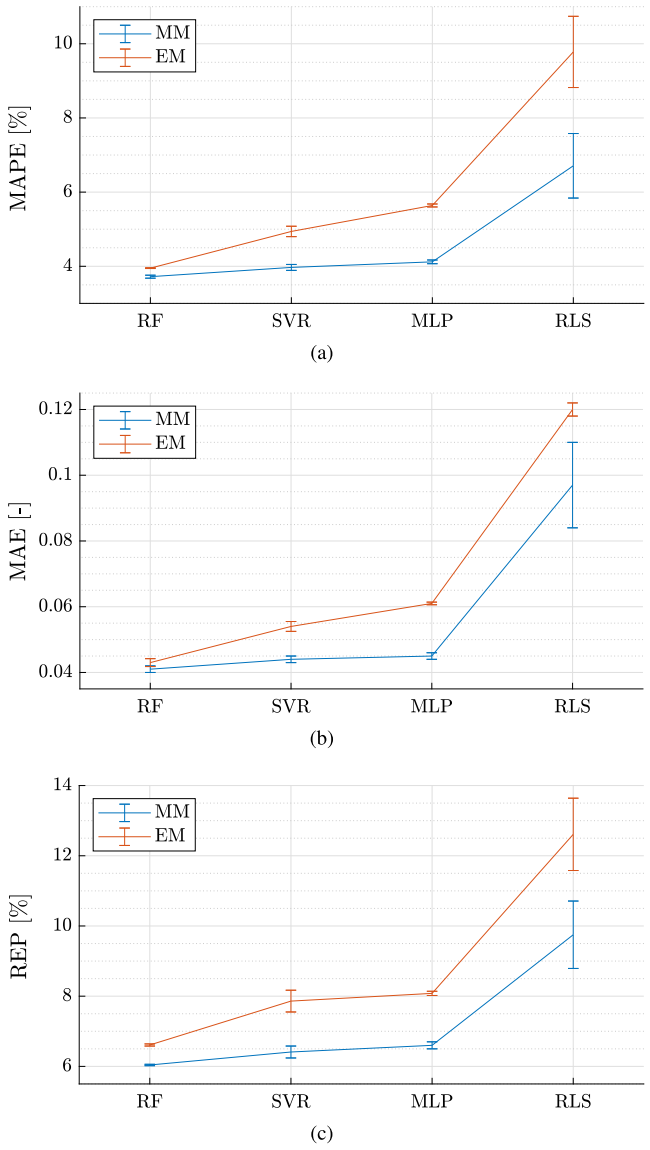

Fig. 15. ML models validation: quantitative metrics (MAPE, MAE, REP) employed to evaluate the performance of all examined algorithms (RF, SVR, MLP, and RLS), on both propulsive modes (MM and EM).

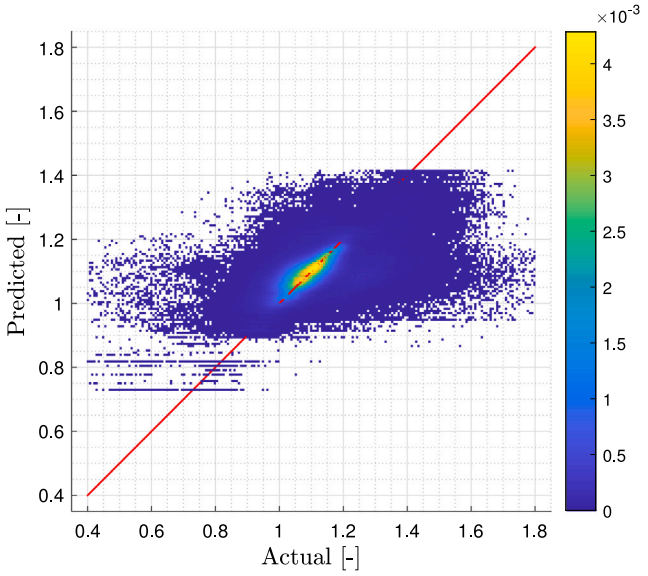

Fig. 16. ML models validation: scatter plot for RF (the best algorithm identified in Section 5.1) on MM (see Table 7).

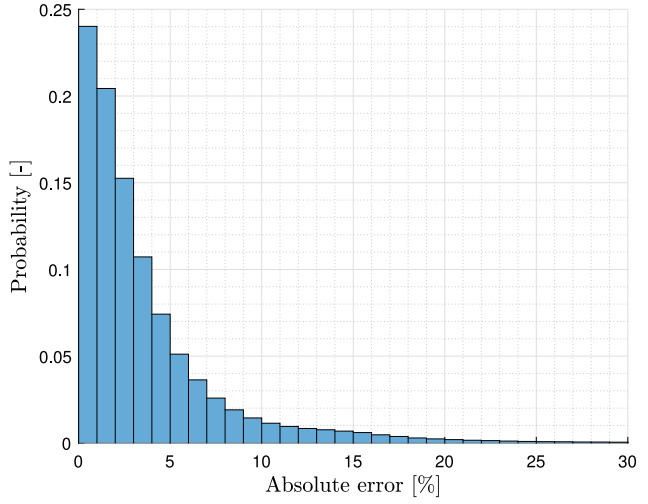

Fig. 17. ML models validation: absolute percentage error histogram of relative frequencies for RF (the best algorithm identified in Section 5.1) on MM (see Table 7).

value equal to 0.976. Results demonstrate the significant improvement in accuracy from integrating ML in our DT. The improvement becomes more apparent on MM as pitch value variates from the nominal value used by the semi-empirical formula. The smaller improvement from using ML on EM is explained by the nominal pitch value resulting from sailing mostly above 50 rpm virtual shaft speed as can be seen in Fig. 7.

6. Results

6.1. Voyage intervals

In the previous section, the capability of the digital twin to predict instant fuel consumption of the vessel and most logged parameters was confirmed. This section provides prediction results over the selected twenty two electrical propulsion and fifty mechanical propulsion voyage intervals that we selected for evaluating the method against real operating conditions. Fig. 20 provides an example of five typical voyage intervals. It provides qualitative means to examine the variation of operational and environmental conditions, that can be assessed using the spread of vessel speed and propeller thrust in corresponding figures. The main characteristics of the selected voyage intervals as duration, average speed, total fuel consumption and carbon intensity, but also the achieved MAPE of the predicted instant fuel consumption and APE of consumed fuel and carbon intensity over the intervals can be found for MM in Table 10 and for EM in Table 11.

Results suggest that the average prediction accuracy over a voyage interval on EM, with a 95% confidence interval, is $1.65 \pm 0.49\%$. At the same time, MAPE of instant fuel consumption is equal to $3.36 \pm 0.35\%$. This shows that increased prediction errors for individual samples of a voyage have a smaller overall impact on a voyage time scale, due to the random sampling behaviour, which is cancelled out over a high amount of samples. This observation is also confirmed for MM with an average prediction accuracy over a voyage of $2.16 \pm 0.35\%$ and an

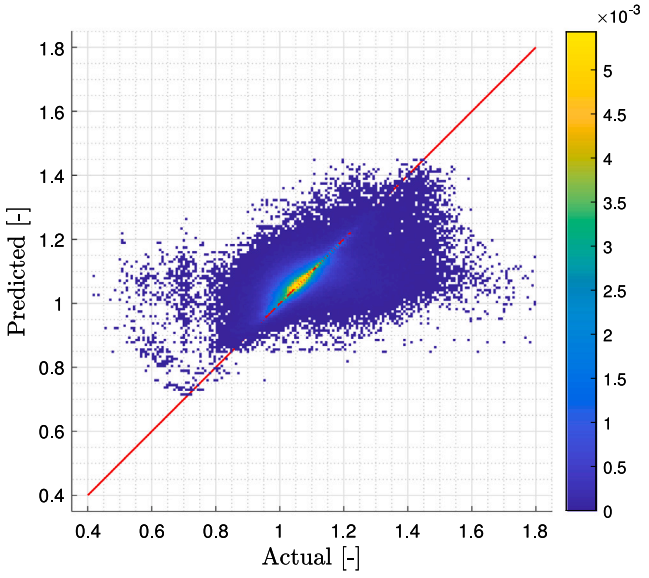

Fig. 18. ML models validation: scatter plot for RF (the best algorithm identified in Section 5.1) on EM (see Table 7).

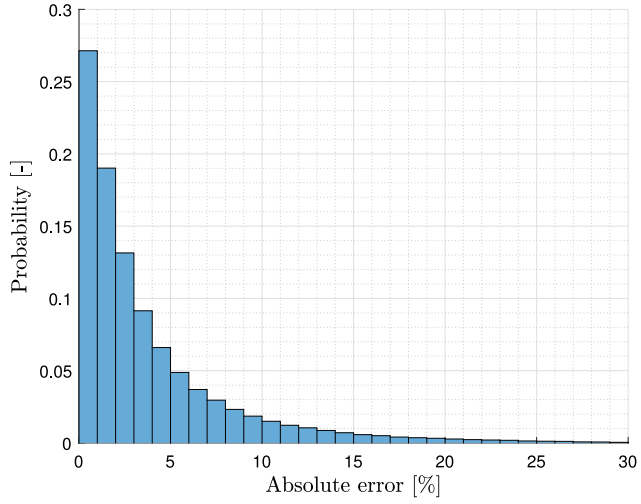

Fig. 19. ML models validation: absolute percentage error histogram of relative frequencies for RF (the best algorithm identified in Section 5.1) on EM (see Table 7).

instant fuel consumption MAPE of 3.79 ± 0.52%. These errors are of the same scale with the accuracy of many fuel consumption sensors at ±1% (Kalikatzarakis et al., 2021), which means that the prediction accuracy is partially limited by the accuracy of the sensors.

6.2. Comparison of electrical and mechanical propulsion

In this section, we provide the results of comparing mechanical and electrical propulsion over ten voyage intervals characterised by non-dynamic conditions when the ship transits between 5 and 10 knots without manoeuvring. During these voyage intervals, the operator can run on either MM or EM. Alternatively, during manoeuvring intervals, which are excluded in this comparison, the operator often has to select MM to have sufficient power available for the manoeuvres. The main constraint of running in EM is the electrical motor's maximum power, which limits the maximum ship speed for these voyage intervals to 10 knots.

Table 8
DT performances using the most performing ML model (RF), assessed over the two operational modes IPMS datasets.

Mechanical mode (MM)				
Feature	MAPE	MAE	REP	R^2
$\dot{m}_{f,tot}$	4.9%	40.1 kg/h	4.7%	0.984
$\dot{m}_{f,gen}$	4.4%	6.8 kg/h	6.0%	0.452
$\dot{m}_{f,e}$	6.2%	38.8 kg/h	5.2%	0.985
eP_{gen}	4.2%	25.1 kW	5.3%	0.481
P_m	–	–		–
M_{psh}	4.4%	3.8 kNm	5.3%	0.977
p	0.5%	0.004	2.2%	0.862
n	0.4%	0.6 rpm	1.2%	0.995
Electrical Mode (EM)				
$\dot{m}_{f,tot}$	3.7%	10.4 kg/h	4.7%	0.913
$\dot{m}_{f,gen}$	3.7%	10.4 kg/h	4.7%	0.913
$\dot{m}_{f,e}$	–	–	–	–
eP_{gen}	3.6%	40.2 kW	4.4%	0.941
P_m	5.3%	12.4 kW	6.3%	0.966
M_{psh}	5.4%	1.4 kNm	6.9%	0.933
p	0.2%	0.002	1.0%	0.338
n	0.6%	0.4 rpm	1.0%	0.995

Table 9
DT performances using the Holtrop and Mennen (1982) semi-empirical formula, assessed over the two operational mode IPMS datasets.

Mechanical mode (MM)				
Feature	MAPE	MAE	REP	R^2
$\dot{m}_{f,tot}$	10.4%	101.3 kg/h	11.0%	0.918
$\dot{m}_{f,gen}$	4.4%	6.8 kg/h	6.0%	0.452
$\dot{m}_{f,e}$	13.1%	102.1 kg/h	12.5%	0.911
eP_{gen}	4.2%	25.1 kW	5.3%	0.481
P_m	–	–		–
M_{psh}	12.9%	13.0 kNm	14.0%	0.839
p	0.5%	0.004	2.2%	0.862
n	0.4%	0.6 rpm	1.2%	0.995
Electrical Mode (EM)				
$\dot{m}_{f,tot}$	5.6%	16.2 kg/h	6.8%	0.818
$\dot{m}_{f,gen}$	5.6%	16.2 kg/h	6.8%	0.818
$\dot{m}_{f,e}$	–	–	–	–
eP_{gen}	6.2%	70.1 kW	7.1%	0.849
P_m	9.9%	26.5 kW	11.9%	0.876
M_{psh}	10.6%	2.8 kNm	12.2%	0.788
p	0.2%	0.002	1.0%	0.338
n	0.6%	0.4 rpm	1.0%	0.995

The comparison of the fuel consumption prediction between MM and EM is presented in Table 12. Fig. 21 provides a visual representation of the result and main influencing parameters. According to the simulation comparison, MM would be, on average, 1.2 ± 1.7% less efficient than EM, and the vessel would consume just 0.67% more fuel in those ten voyage intervals combined. Nevertheless, it appears that higher mean sea margin and speed favours MM. It is interesting to compare these results with the results of previous work by Vasilikis et al. (2022). In the data analysis performed on the same vessel's data, electrical propulsion appeared less efficient, but this was the case for the specific operational and environmental conditions for each mode selected, thus not comparing under similar conditions. Hence, we conclude that simulation of the vessel's energy performance on the exact same voyage intervals demonstrates that there are no clear energy efficiency benefits from sailing on one of the two operational modes, while many other influencing parameters can have a more significant impact on attained energy performance.

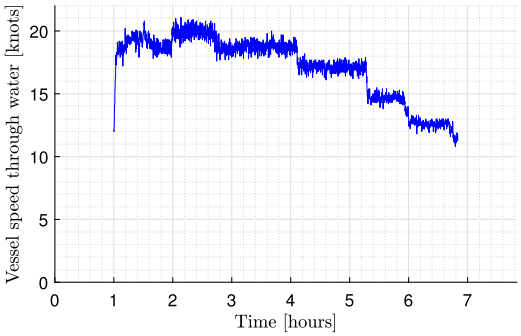

(a) Interval No 3 (MM), speed over time.

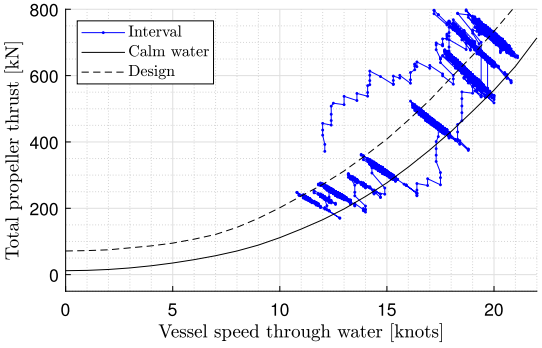

(b) Interval No 3 (MM), thrust over speed.

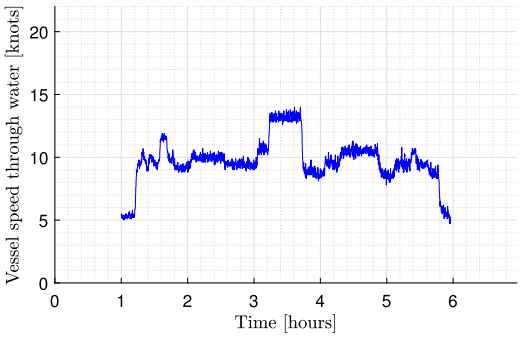

(c) Interval No 4 (MM), speed over time.

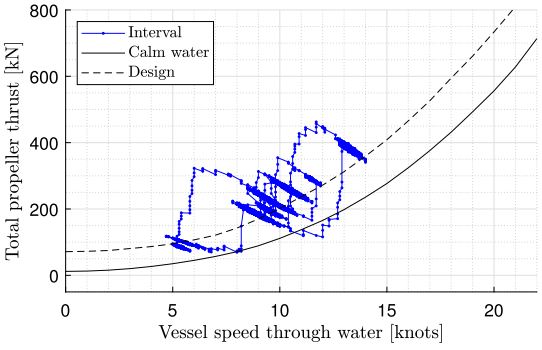

(d) Interval No 4 (MM), thrust over speed.

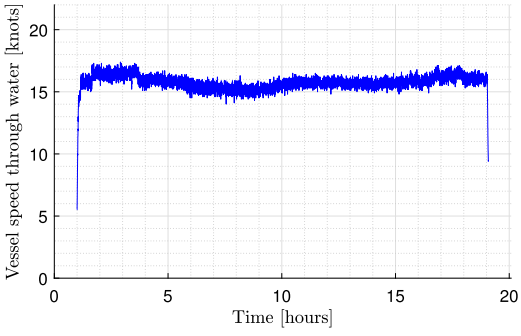

(e) Interval No 15 (MM), speed over time.

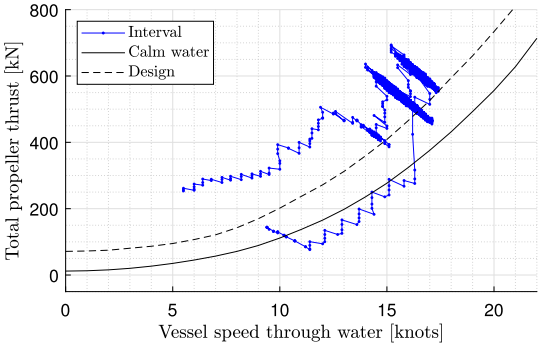

(f) Interval No 15 (MM), thrust over speed.

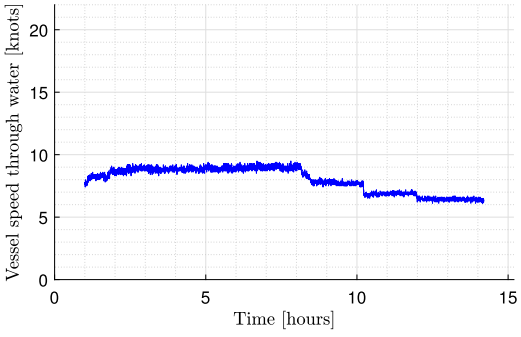

(g) Interval No 6 (EM), speed over time.

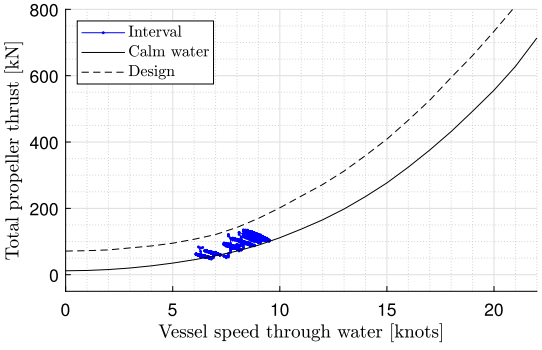

(h) Interval No 6 (EM), thrust over speed.

Fig. 20. Typical voyage intervals.

Table 10
Comparison between the MAPE of the instant fuel consumption and the APE of the amount of fuel and carbon intensity over the selected mechanical mode (MM) voyage intervals.

	Duration [hours]	Mean speed [knots]	$M_{f,tot}$ [tons]	Carbon intensity [kgCO2\nm]	MAPE $\dot{m}_{f,tot}$ [%]	APE $M_{f,tot}$/CI [%]
1	10.2	12.2	6.2	160.9	5.82	2.73
2	6.2	15.7	6.2	201.8	4.62	3.82
3	5.8	17.2	8.1	258.8	4.40	2.54
4	5.0	9.7	2.4	159.4	11.18	1.74
5	8.8	10.3	4.8	169.9	7.07	0.69
6	5.8	18.7	11.5	342.5	2.77	1.41
7	5.4	17.0	7.3	254.4	4.30	4.06
8	9.1	18.7	16.4	308.8	3.32	3.00
9	13.5	17.9	21.8	289.4	2.80	2.03
10	7.0	13.6	5.4	182.8	2.81	0.91
11	16.4	17.5	24.7	274.8	3.20	2.65
12	9.0	17.8	16.3	325.2	2.21	1.85
13	13.6	16.3	17.9	258.9	1.99	0.97
14	18.5	15.2	22.2	253.2	2.79	1.72
15	18.1	15.8	24.1	271.7	2.26	1.60
16	5.0	11.5	3.3	182.5	9.56	1.53
17	16.3	13.6	16.6	238.8	4.79	1.49
18	8.3	13.0	7.3	214.1	3.06	0.59
19	25.8	13.4	24.1	224.1	3.52	2.30
20	10.8	15.7	15.1	284.6	2.83	0.97
21	14.5	14.4	14.8	227.0	2.00	0.92
22	3.9	14.8	4.3	241.1	1.97	0.92
23	12.3	15.1	13.6	234.0	2.08	1.81
24	11.7	14.9	12.7	233.8	2.30	1.62
25	13.3	12.9	9.4	175.7	4.61	2.29
26	10.8	13.3	7.4	165.7	5.23	2.58
27	9.6	15.5	9.8	211.5	3.37	2.65
28	11.4	17.1	14.5	239.8	1.89	0.33
29	7.7	14.4	6.1	178.8	2.78	0.82
30	10.6	16.4	13.6	251.8	2.83	1.40
31	10.6	15.9	14.0	267.8	4.36	4.25
32	13.4	14.3	13.2	222.3	6.73	4.05
33	7.9	15.8	8.6	220.1	3.58	2.07
34	20.0	14.4	16.9	188.0	3.29	0.24
35	25.2	18.2	39.3	275.2	2.82	2.56
36	15.8	14.0	11.7	170.0	4.24	3.90
37	23.0	15.0	20.9	194.5	3.48	2.70
38	24.5	15.2	22.1	190.7	2.50	1.94
39	14.6	15.9	15.2	210.6	3.37	2.16
40	12.4	16.6	16.2	252.5	3.21	3.00
41	4.7	16.8	6.1	247.6	1.95	0.61
42	17.8	16.7	23.1	249.7	2.08	0.39
43	15.7	17.1	21.2	254.0	2.40	1.42
44	23.2	16.9	29.0	236.3	4.47	4.42
45	12.2	16.4	13.9	220.9	4.81	4.79
46	8.3	14.9	7.6	196.1	4.39	4.37
47	16.9	14.7	14.8	190.6	4.43	3.79
48	15.7	13.9	13.0	191.3	3.71	1.59
49	28.1	15.1	27.8	209.3	4.63	1.96
50	10.0	18.8	16.8	285.0	4.69	3.87
Average					3.79 ± 0.52	2.16 ± 0.35

Table 11
Comparison between the MAPE of the instant fuel consumption and the APE of the amount of fuel and carbon intensity over the selected electrical mode (EM) voyage intervals.

	Duration [hours]	Mean speed [knots]	$M_{f,tot}$ [tons]	Carbon intensity [kgCO2\nm]	MAPE $\dot{m}_{f,tot}$ [%]	APE $M_{f,tot}$/CI [%]
1	5.3	9.3	1.7	110.1	4.02	3.23
2	9.1	6.2	1.9	109.2	3.88	1.19
3	7.1	7.3	1.9	119.8	3.75	0.46
4	8.0	7.9	2.2	109.8	3.95	3.46
5	10.5	7.4	3.0	123.2	4.08	3.14
6	13.2	8.0	3.7	111.0	2.91	2.27
7	4.7	7.8	1.3	119.3	3.20	2.25
8	9.8	5.3	2.1	127.9	4.75	3.42
9	10.1	7.4	2.7	118.2	2.58	2.29
10	5.3	7.4	1.5	118.2	2.54	1.82
11	13.1	7.0	4.5	157.6	1.92	0.83
12	21.2	8.0	7.5	142.5	4.43	3.25
13	10.1	8.1	3.5	138.7	4.31	0.14
14	12.6	6.4	3.5	140.0	3.38	1.31
15	8.5	7.1	2.5	134.7	2.32	0.90
16	6.8	6.8	2.0	136.3	2.88	1.83
17	11.3	4.9	2.5	143.2	3.77	0.93
18	9.2	6.3	2.3	129.6	3.59	0.23
19	11.4	5.9	2.9	135.5	3.24	1.03
20	22.6	6.2	5.8	132.7	2.77	0.73
21	21.0	7.1	5.6	120.5	3.55	0.85
22	13.7	8.0	4.2	124.7	2.03	0.69
Average					3.36 ± 0.35	1.65 ± 0.49

Table 12
Total fuel consumption prediction on mechanical (MM) and electrical mode (EM) on selected electrical propulsion voyage intervals.

	Mean speed [knots]	Mean SM [%]	Actual EM [tons]	Predicted EM [tons]	Predicted MM [tons]	MM to EM [%]
1	9.3	24	1.67	1.72	1.78	+3.1
6	8.0	26	3.65	3.74	3.79	+1.6
7	7.8	55	1.35	1.38	1.40	+1.3
9	7.4	46	2.74	2.80	2.90	+3.4
10	7.4	43	1.46	1.49	1.53	+2.6
11	7.0	133	4.51	4.47	4.33	−3.3
13	8.1	85	3.54	3.54	3.45	−2.6
14	6.4	105	3.53	3.58	3.63	+1.5
15	7.1	88	2.53	2.55	2.57	+1.0
18	6.3	75	2.35	2.34	2.42	+3.3
Total accumulated			27.33	27.61	27.80	+0.7
Average						$+1.2 \pm 1.7$

7. Conclusions and recommendations

This work proposes a method to evaluate and predict carbon intensity in actual operational and environmental conditions. This method can be used to provide insight and guidance to improvements in the operation and design of ship propulsion and power systems to achieve more energy efficient designs and reduce the carbon intensity of ship operation over the lifetime of a vessel. This paper proposes a novel digital twin that accurately predicts the fuel consumption and carbon intensity of mechanical, electrical, and hybrid propulsion systems under the aggregate effect of operational and environmental uncertainties. A combined approach with first principle steady state models and machine learning models allows us to predict instantaneous fuel consumption with an accuracy of less than 5% MAPE and carbon intensity over voyage intervals within 2.5% at a confidence interval of 95% for the case study OPV. The use of machine learning algorithms contributes to improving prediction accuracy on the scale of 40 to 50%.

This work provides proof that steady state models can accurately predict fuel consumption and carbon footprint during both dynamic manoeuvring and constant speed operations. The prediction accuracy of the total amount of consumed fuel and carbon intensity over a sufficiently long voyage is higher than the point wise accuracy of the model. A combination of first principle and machine learning models can be used to overcome uncertainty due to inaccurate sensor readings and manufacturers' data, the scale effect of hull and propeller measurements, true operational conditions, and dynamic operational decisions. We expect using data from a thrust sensor can provide even more accurate predictions, as thrust measurement enables separating the effect of uncertainty due to the environmental conditions and scale effects from the effect of uncertainties in the efficiency of the propulsion plant due to inaccurate manufacturers' data and sensor readings.

The proposed method can be used to make accurate comparisons between different operating modes for real operating profiles represented by typical voyages under various conditions. The case study patrol

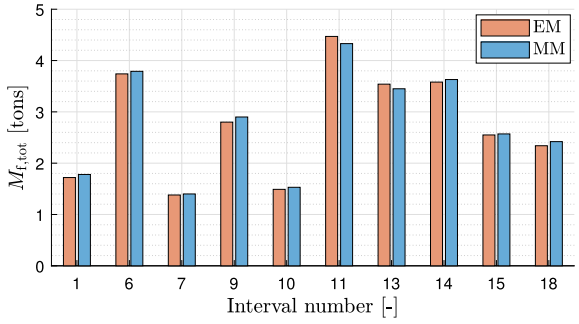

(a) Total fuel consumption.

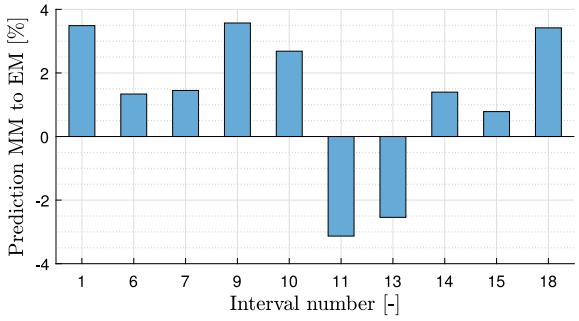

(b) Prediction difference between MM and EM.

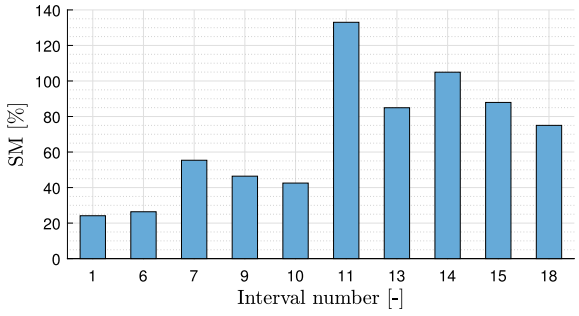

(c) Mean sea margin.

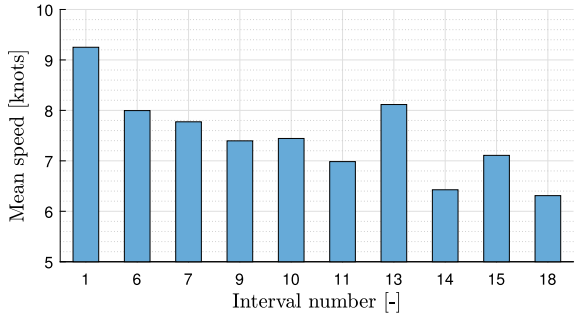

(d) Mean speed.

Fig. 21. Comparison of MM and EM energy performance on the selected ten EM voyage intervals.

vessel's results indicate that electrical propulsion does not provide statistically significant fuel and carbon savings, even though electrical mode can prevent the main diesel engines from running at low speed and can reduce noise levels. This result emphasises the need to evaluate and predict carbon intensity with models that account for operational and environmental conditions. In future work, we intend to demonstrate how the method can be applied to the evaluation of propulsion and power systems configuration modifications, but also to the evaluation of alternative design options for ships with a similar operating profile.

Declaration of competing interest

The authors declare that they have no known competing financial interests or personal relationships that could have appeared to influence the work reported in this paper.

Data availability

Data will be made available on request.

Acknowledgements

This work is supported by The Netherlands Organisation for Scientific Research (NWO) [Nederlandse organisatie voor Wetenschappelijk Onderzoek] project 'AssetDrive: Translating maintenance analysis and operational data to enhanced ship system design and performance contracts' (ALWTW.016.042). Moreover, this work used the increased computing capabilities of the Delft Supercomputer (Phase 1) (Delft High Performance Computing Centre (DHPC), 2022).

References

Aggarwal, C.C., 2015. Data Mining: The Textbook. Springer.

Al-Falahi, Monaaf D.A., Nimma, Kutaiba S., Jayasinghe, Shantha D.G., Enshaei, Hossein, Guerrero, Josep M., 2018. Power management optimization of hybrid power systems in electric ferries. Energy Convers. Manage. 172, 50–66. http://dx.doi.org/10.1016/j.enconman.2018.07.012.

Aldous, L., Smith, T., Bucknall, R., Thompson, P., 2015. Uncertainty analysis in ship performance monitoring. Ocean Eng. 110, 29–38. http://dx.doi.org/10.1016/j.oceaneng.2015.05.043.

Ancona, M.A., Baldi, F., Bianchi, M., Branchini, L., Melino, F., Peretto, A., Rosati, J., 2018. Efficiency improvement on a cruise ship: Load allocation optimization. Energy Convers. Manage. 164, 42–58. http://dx.doi.org/10.1016/j.enconman.2018.02.080.

Avgouleas, Kyriakos, Sclavounos, Paul D., 2014. Fuel-efficient ship routing. Nausivios Chora C Natur. Sci. Math. 5, 39–72.

Baldi, Francesco, 2016. Modelling, Analysis and Optimisation of Ship Energy Systems (Ph.D. thesis). Department of Shipping and Marine Technology, Chalmers University of Technology, Gothenburg, Sweden.

Baldi, F., Johnson, H., Gabrielii, C., Andersson, K., 2015a. Energy and exergy analysis of ship energy systems - The case study of a chemical tanker. Int. J. Thermodyn. 18 (2), 82–93. http://dx.doi.org/10.5541/ijot.70299.

Baldi, Francesco, Larsen, Ulrik, Gabrielii, Cecilia, 2015b. Comparison of different procedures for the optimisation of a combined Diesel engine and organic Rankine cycle system based on ship operational profile. Ocean Eng. 110, 85–93. http://dx.doi.org/10.1016/j.oceaneng.2015.09.037.

Barsali, Stefano, Miulli, Carmine, Possenti, Andrea, 2004. A control strategy to minimize fuel consumption of series hybrid electric vehicles. IEEE Trans. Energy Convers. 19 (1), 187–195. http://dx.doi.org/10.1109/TEC.2003.821862.

Bishop, C.M., 1995. Neural Networks for Pattern Recognition. Oxford University Press.

Bouman, Evert A., Lindstad, Elizabeth, Rialland, Agathe I., Strømman, Anders H., 2017. State-of-the-art technologies, measures, and potential for reducing GHG emissions from shipping – A review. Transp. Res. D 52, 408–421. http://dx.doi.org/10.1016/j.trd.2017.03.022.

Bulten, N., 2016. With numerical simulations to more efficient ship designs. In: Proceedings RINA Energy Efficient Ships Conference. London, UK.

Carlton, J.S., 2019. Marine Propellers and Propulsion. Butterworth-Heinemann, An imprint of Elsevier.

Coraddu, Andrea, Figari, Massimo, Savio, Stefano, 2014. Numerical investigation on ship energy efficiency by Monte Carlo simulation. Proc. Inst. Mech. Eng. M 228 (3), 220–234. http://dx.doi.org/10.1177/1475090214524184.

Coraddu, A., Kalikatzarakis, M., Oneto, L., Meijn, G.J., Godjevac, M., Geertsma, R.D., 2018. Ship diesel engine performance modelling with combined physical and machine learning approach. In: Proceedings of the International Ship Control Systems Symposium. ISCSS.

Coraddu, A., Kalikatzarakis, M., Theotokatos, G., Geertsma, R., Oneto, L., 2021. Engine modeling and simulation. Energy, environment, and sustainability. In: Agarwal, A.K., Kumar, D., Sharma, N., Sonawane, U. (Eds.), Physical and Data-Driven Models Hybridisation for Modelling the Dynamic State of a Four-Stroke Marine Diesel Engine. Springer, Singapore, pp. 145–193. http://dx.doi.org/10.1007/978-981-16-8618-4_6.

Coraddu, Andrea, Lim, Serena, Oneto, Luca, Pazouki, Kayvan, Norman, Rose, Murphy, Alan John, 2019. A novelty detection approach to diagnosing hull and propeller fouling. Ocean Eng. 176, 65–73. http://dx.doi.org/10.1016/j.oceaneng.2019.01.054.

Coraddu, Andrea, Oneto, Luca, Baldi, Francesco, Anguita, Davide, 2017. Vessels fuel consumption forecast and trim optimisation: A data analytics perspective. Ocean Eng. 130, 351–370. http://dx.doi.org/10.1016/j.oceaneng.2016.11.058.

Cybenko, G., 1989. Approximation by superpositions of a sigmoidal function. Math. Control Signals Systems 2 (4), 303–314.

Damerius, R., Schubert, A.U., Rethfeldt, C., Finger, G., Fischer, S., Milbradt, G., Kurowski, M., Gluch, M., Jeinsch, T., 2022. Consumption-reduced manual and automatic manoeuvring with conventional vessels. J. Mar. Eng. Technol. 1–12. http://dx.doi.org/10.1080/20464177.2022.2154666.

Dedes, Eleftherios K., Hudson, Dominic A., Turnock, Stephen R., 2012. Assessing the potential of hybrid energy technology to reduce exhaust emissions from global shipping. Energy Policy 40, 204–218. http://dx.doi.org/10.1016/j.enpol.2011.09.046.

Dedes, Eleftherios K., Hudson, Dominic A., Turnock, Stephen R., 2016. Investigation of Diesel hybrid systems for fuel oil reduction in slow speed ocean going ships. Energy 114, 444–456. http://dx.doi.org/10.1016/j.energy.2016.07.121.

Delft High Performance Computing Centre (DHPC), 2022. DelftBlue supercomputer (Phase 1). https://www.tudelft.nl/dhpc/ark:/44463/DelftBluePhase1.

Diez, Matteo, Campana, Emilio F., Stern, Frederick, 2018. Stochastic optimization methods for ship resistance and operational efficiency via CFD. Struct. Multidiscip. Optim. 57, 735–758.

Esmailian, Ehsan, Steen, Sverre, Koushan, Kourosh, 2022. Ship design for real sea states under uncertainty. Ocean Eng. 266, 113127. http://dx.doi.org/10.1016/j.oceaneng.2022.113127.

Fan, Ailong, Yan, Xinping, Bucknall, Richard, Yin, Qizhi, Ji, Sheng, Liu, Yuanchang, Song, Rui, Chen, Xiaping, 2020. A novel ship energy efficiency model considering random environmental parameters. J. Mar. Eng. Technol. 19 (4), 215–228. http://dx.doi.org/10.1080/20464177.2018.1546644.

Farag, Yasser B.A., Ölçer, Aykut I., 2020. The development of a ship performance model in varying operating conditions based on ANN and regression techniques. Ocean Eng. 198, 106972. http://dx.doi.org/10.1016/j.oceaneng.2020.106972.

Fernández-Delgado, M., Cernadas, E., Barro, S., Amorim, D., 2014. Do we need hundreds of classifiers to solve real world classification problems? J. Mach. Learn. Res. 15 (1), 3133–3181.

Geertsma, R.D., Negeborn, R.R., Visser, K., Loonstijn, M.A., Hopman, J.J., 2017. Pitch control for ships with diesel mechanical and hybrid propulsion: Modelling, validation and performance quantification. Appl. Energy 206, 1609–1631. http://dx.doi.org/10.1016/j.apenergy.2017.09.103.

Geertsma, R.D., Visser, K., Negeborn, R.R., 2018. Adaptive pitch control for ships with diesel mechanical and hybrid propulsion. Appl. Energy 228, 2490–2509. http://dx.doi.org/10.1016/j.apenergy.2018.07.080.

Georgescu, Ioana, Godjevac, Milinko, Visser, Klaas, 2018. Efficiency constraints of energy storage for on-board power systems. Ocean Eng. 162, 239–247. http://dx.doi.org/10.1016/j.oceaneng.2018.05.004.

Gkerekos, Christos, Lazakis, Iraklis, Theotokatos, Gerasimos, 2019. Machine learning models for predicting ship main engine Fuel Oil Consumption: A comparative study. Ocean Eng. 188, 106282. http://dx.doi.org/10.1016/j.oceaneng.2019.106282.

Godjevac, M., Drijver, J., de Vries, L., Stapersma, D., 2015. Evaluation of losses in maritime gearboxes. Proceedings of the IMechE, Part M: Journal of Engineering for the Maritime Environment 1–16. http://dx.doi.org/10.1177/1475090215613814.

Goodfellow, I., Bengio, Y., Courville, A., Bengio, Y., 2016. Deep Learning. MIT press Cambridge.

Grieves, Michael, Vickers, John, 2017. Digital twin: Mitigating unpredictable, undesirable emergent behavior in complex systems. In: Kahlen, Franz-Josef, Flumerfelt, Shannon, Alves, Anabela (Eds.), Transdisciplinary Perspectives on Complex Systems: New Findings and Approaches. Springer International Publishing, Cham, pp. 85–113. http://dx.doi.org/10.1007/978-3-319-38756-7_4.

Gypa, Ioli, Jansson, Marcus, Gustafsson, Robert, Werner, Sofia, Bensow, Rickard, 2023. Controllable-pitch propeller design process for a wind-powered car-carrier optimising for total energy consumption. Ocean Eng. 269, 113426. http://dx.doi.org/10.1016/j.oceaneng.2022.113426.

Haseltalab, Ali, Botto, Miguel Ayala, Negenborn, Rudy R., 2019. Model predictive DC voltage control for all-electric ships. Control Eng. Pract. 90, 133–147. http://dx.doi.org/10.1016/j.conengprac.2019.06.018.

Haseltalab, Ali, Negenborn, Rudy R., 2019. Model predictive maneuvering control and energy management for all electric autonomous ships. Appl. Energy 251, http://dx.doi.org/10.1016/j.apenergy.2019.113308.

Holtrop, J., 1984. A statistical RE-Analysis of resistance and propulsion data. Int. Shipbuild. Prog. 31 (363), 272–276.

Holtrop, J., Mennen, G.G.J., 1982. An approximate power prediction method. Int. Shipbuild. Prog. 29, 166–171.

Hountalas, Dimitrios T., 2000. Prediction of marine diesel engine performance under fault conditions. Applied Thermal Engineering 20, 1753–1783. http://dx.doi.org/10.1016/S1359-4311(00)00006-5.

Huang, Luofeng, Pena, Blanca, Liu, Yuanchang, Anderlini, Enrico, 2022. Machine learning in sustainable ship design and operation: A review. Ocean Eng. 266, 112907. http://dx.doi.org/10.1016/j.oceaneng.2022.112907.

Huijgens, Lode, Vrijdag, Arthur, Hopman, Hans, 2022. Hardware in the loop experiments on the interaction between a diesel-mechanical propulsion system and a ventilating propeller. J. Mar. Eng. Technol. 1–13. http://dx.doi.org/10.1080/20464177.2022.2138736.

IMO, 2020. Fourth IMO GHG Study 2020. Technical Report, International Maritime Organization.

IPCC, 2021. Summary for policymakers. In: Masson-Delmotte, V., Zhai, P., Pirani, A., Connors, S.L., Péan, C., Berger, S., Caud, N., Chen, Y., Goldfarb, L., Gomis, M.I., Huang, M., Leitzell, K., Lonnoy, E., Matthews, J.B.R., Maycock, T.K., Waterfield, T., Yelekçi, O., Yu, R., Zhou, B. (Eds.), Climate Change 2021: The Physical Science Basis. Contribution of Working Group I to the Sixth Assessment Report of the Intergovernmental Panel on Climate Change. Cambridge University Press.

ITTC, 2014. Recommended Procedures and Guidelines - 1978 ITTC Performance Prediction Method 7.5-02-03-01.4. Technical Report, International Towing Tank Conference.

Kalikatzarakis, Miltiadis, Coraddu, Andrea, Theotokatos, Gerasimos, Oneto, Luca, 2021. Development of a zero-dimensional model and application on a medium-speed marine four-stroke diesel engine. In: Proceedings of MOSES2021 Conference.

Kalikatzarakis, M., Geertsma, R.D., Boonen, E.J., Visser, K., Negenborn, R.R., 2018. Ship energy management for hybrid propulsion and power supply with shore charging. Control Eng. Pract. 76, 133–154. http://dx.doi.org/10.1016/j.conengprac.2018.04.009.

Karagiannidis, Pavlos, Themelis, Nikos, 2021. Data-driven modelling of ship propulsion and the effect of data pre-processing on the prediction of ship fuel consumption and speed loss. Ocean Eng. 108616. http://dx.doi.org/10.1016/j.oceaneng.2021.108616.

Keerthi, S.S., Lin, C.J., 2003. Asymptotic behaviors of support vector machines with Gaussian kernel. Neural Comput. 15 (7), 1667–1689.

Lindstad, Elizabeth, Borgen, Henning, Eskeland, Gunnar S., Paalson, Christopher, Psaraftis, Harilaos, Turan, Osman, 2019. The need to amend IMO's EEDI to include a threshold for performance in waves (realistic sea conditions) to achieve the desired ghg reductions. Sustainability 11 (13), 3668. http://dx.doi.org/10.3390/su11133668.

Lu, Ruihua, Turan, Osman, Boulougouris, Evangelos, Banks, Charlotte, Incecik, Atilla, 2015. A semi-empirical ship operational performance prediction model for voyage optimization towards energy efficient shipping. Ocean Eng. 110, 18–28. http://dx.doi.org/10.1016/j.oceaneng.2015.07.042.

MAN Energy Solutions, 2018. Basic principles of ship propulsion optimisation of hull, propeller, and engine interactions for maximum efficiency.

Mauro, F., Kana, A.A., 2023. Digital twin for ship life-cycle: A critical systematic review. Ocean Eng. 269, 113479. http://dx.doi.org/10.1016/j.oceaneng.2022.113479.

MEPC, 2011. Resolution MEPC.203(62) ANNEX 19 Amendments to the Annex of the Protocol of 1997 to Amend the International Convention for the Prevention of Pollution from Ships, 1973, as Modified by the Protocol of 1978 Relating Thereto (Inclusion of Regulations on Energy Efficiency for Ships in MARPOL Annex VI). Technical Report, International Maritime Organization.

MEPC, 2014. Resolution MEPC.245(66) ANNEX 5 Guidelines on the Method of Calculation of the Attained Energy Efficiency Design Index (EEDI) for New Ships. Technical Report, International Maritime Organization.

MEPC, 2018. Resolution MEPC.304(72) ANNEX 11 Initial IMO Strategy on Reduction of GHG Emissions from Ships. Technical Report, International Maritime Organization.

MEPC, 2021a. Resolution MEPC.333(76) ANNEX 7 2021 Guidelines on the Method of Calculation of the Attained Energy Efficiency Existing Ship Index (EEXI). Technical Report, International Maritime Organization.

MEPC, 2021b. Resolution MEPC.336(76) ANNEX 10 2021 Guidelines on Operational Carbon Intensity Indicators and the Calculation Methods (CII Guidelines, G1). Technical Report, International Maritime Organization.

Moreno-Gutiérrez, Juan, Calderay, Fátima, Saborido, Nieves, Boile, Maria, Valero, Rafael Rodríguez, Durán-Grados, Vanesa, 2015. Methodologies for estimating shipping emissions and energy consumption: A comparative analysis of current methods. Energy 86, 603–616. http://dx.doi.org/10.1016/j.energy.2015.04.083.

Naser, M.Z., Alavi, A.H., 2021. Error metrics and performance fitness indicators for artificial intelligence and machine learning in engineering and sciences. Archit. Struct. Constr. 1–19. http://dx.doi.org/10.1007/s44150-021-00015-8.

Nikolopoulos, Lampros, Boulougouris, Evangelos, 2020. A novel method for the holistic, simulation driven ship design optimization under uncertainty in the big data era. Ocean Eng. 218, 107634. http://dx.doi.org/10.1016/j.oceaneng.2020.107634.

Oneto, Luca, 2020. Model Selection and Error Estimation in a Nutshell. Springer.

Parkes, A.I., Sobey, A.J., Hudson, D.A., 2018. Physics-based shaft power prediction for large merchant ships using neural networks. Ocean Eng. 166, 92–104. http://dx.doi.org/10.1016/j.oceaneng.2018.07.060.

Rosenblatt, F., 1958. The perceptron: a probabilistic model for information storage and organization in the brain. Psychol. Rev. 65 (6), 386.

Rumelhart, D.E., Hinton, Geoffrey. E., Williams, R.J., 1986. Learning representations by back-propagating errors. Nature 323 (6088), 533–536.

Sainani, Kristin L., 2016. The value of scatter plots. Phys. Med. Rehabil. 1213–1217. http://dx.doi.org/10.1016/j.pmrj.2016.10.018.

Sakalis, George N., Frangopoulos, Christos A., 2018. Intertemporal optimization of synthesis, design and operation of integrated energy systems of ships: General method and application on a system with Diesel main engines. Appl. Energy 226, 991–1008. http://dx.doi.org/10.1016/j.apenergy.2018.06.061.

Scholkopf, B., 2001. The kernel trick for distances. In: Advances in Neural Information Processing Systems. pp. 301–307.

Shalev-Shwartz, S., Ben-David, S., 2014. Understanding Machine Learning: From Theory to Algorithms. Cambridge University Press.

Shawe-Taylor, J.S., Cristianini, N., 2004. Kernel Methods for Pattern Analysis. Cambridge University Press.

Shi, W., Grimmelius, H.T., Stapersma, D., 2010. Analysis of ship propulsion system behaviour and the impact on fuel consumption. Int. Shipbuild. Prog. 57 (1–2), 35–64. http://dx.doi.org/10.3233/ISP-2010-0062.

Shu, Gequn, Liu, Peng, Tian, Hua, Wang, Xuan, Jing, Dongzhan, 2017. Operational profile based thermal-economic analysis on an Organic Rankine cycle using for harvesting marine engine's exhaust waste heat. Energy Convers. Manage. 146, 107–123. http://dx.doi.org/10.1016/j.enconman.2017.04.099.

Stapersma, Douwe, Klein Woud, Hans, 2005. Matching propulsion engine with propulsor. J. Mar. Eng. Technol. 4 (2), 25–32. http://dx.doi.org/10.1080/20464177.2005.11020189.

Sui, Congbiao, de Vos, Peter, Stapersma, Douwe, Visser, Klaas, Ding, Yu, 2020. Fuel consumption and emissions of ocean-going cargo ship with hybrid propulsion and different fuels over voyage. J. Mar. Sci. Eng. 8 (588), 588. http://dx.doi.org/10.3390/jmse8080588.

Sui, Congbiao, Stapersma, Douwe, Visser, Klaas, de Vos, Peter, Ding, Yu, 2019. Energy effectiveness of ocean-going cargo ship under various operating conditions. Ocean Eng. 190, http://dx.doi.org/10.1016/j.oceaneng.2019.106473.

Tadros, M., Ventura, M., Guedes Soares, C., 2022. Optimization procedures for a twin controllable pitch propeller of a ROPAX ship at minimum fuel consumption. J. Mar. Eng. Technol. 1–9. http://dx.doi.org/10.1080/20464177.2022.2106623.

Taylor, D.W., 1910. The Speed and Power of Ships a Manual of Marine Propulsion. John Wiley & sons, inc.

Tillig, Fabian, Ringsberg, Jonas W., Mao, Wengang, Ramne, Bengt, 2018. Analysis of uncertainties in the prediction of ships' fuel consumption – from early design to operation conditions. Ships Offshore Struct. 13 (sup1), 13–24. http://dx.doi.org/10.1080/17445302.2018.1425519.

Trivyza, Nikoletta L., Rentizelas, Athanasios, Theotokatos, Gerasimos, 2018. A novel multi-objective decision support method for ship energy systems synthesis to enhance sustainability. Energy Convers. Manage. 168, 128–149. http://dx.doi.org/10.1016/j.enconman.2018.04.020.

Trivyza, Nikoletta L., Rentizelas, Athanasios, Theotokatos, Gerasimos, 2020. A comparative analysis of EEDI versus lifetime CO2 emissions. J. Mar. Sci. Eng. 8 (1), 61. http://dx.doi.org/10.3390/jmse8010061.

Trodden, D.G., Murphy, A.J., Pazouki, K., Sargeant, James, 2015. Fuel usage data analysis for efficient shipping operations. Ocean Eng. 110, 75–84. http://dx.doi.org/10.1016/j.oceaneng.2015.09.028.

van Straten, O.F.A., de Boer, M.J., 2012. Optimum propulsion engine configuration from fuel economic point of view. In: Proceedings of the 11th International Naval Engineering Conference and Exhibition. INEC, http://dx.doi.org/10.24868/issn.2515-818X.2020.066.

Vasilikis, Nikolaos I., Geertsma, Rinze D., Visser, Klaas, 2022. Operational data-driven energy performance assessment of ships: the case study of a naval vessel with hybrid propulsion. J. Mar. Eng. Technol. http://dx.doi.org/10.1080/20464177.2022.2058690.

Vergara, Julio, McKesson, Chris, Walczak, Magdalena, 2012. Sustainable energy for the marine sector. Energy Policy 49, 333–345. http://dx.doi.org/10.1016/j.enpol.2012.06.026.

Vrijdag, Arthur, 2014. Estimation of uncertainty in ship performance predictions. J. Mar. Eng. Technol. 13 (3), 45–55. http://dx.doi.org/10.1080/20464177.2014.11658121.

Vrijdag, Arthur, Boonen, Erik-Jan, Lehne, Markus, 2018. Effect of uncertainty on techno-economic trade-off studies: ship power and propulsion concepts. J. Mar. Eng. Technol. 18 (3), 122–133. http://dx.doi.org/10.1080/20464177.2018.1507430.

Wainberg, M., Alipanahi, B., Frey, B.J., 2016. Are random forests truly the best classifiers? J. Mach. Learn. Res. 17 (1), 3837–3841.

Wolpert, D.H., 2002. The supervised learning no-free-lunch theorems. Soft Comput. Ind. 25–42.

Zahedi, Bijan, Norum, Lars E., Ludvigsen, Kristine B., 2014. Optimized efficiency of all-electric ships by dc hybrid power systems. J. Power Sources 255, 341–354. http://dx.doi.org/10.1016/j.jpowsour.2014.01.031.

Zhang, Chi, Zhang, Di, Zhang, Mingyang, Mao, Wengang, 2019. Data-driven ship energy efficiency analysis and optimization model for route planning in ice-covered Arctic waters. Ocean Eng. 186, 106071. http://dx.doi.org/10.1016/j.oceaneng.2019.05.053.

Zhou, Zhi-Hua, 2012. Ensemble Methods: Foundations and Algorithms. CRC Press.

Zhou, Min, Jin, Hui, Wang, Wenshuo, 2016. A review of vehicle fuel consumption models to evaluate eco-driving and eco-routing. Transp. Res. D 49, 203–218. http://dx.doi.org/10.1016/j.trd.2016.09.008.

Zhu, Jianyun, Chen, Li, Wang, Bin, Xia, Lijuan, 2018. Optimal design of a hybrid electric propulsive system for an anchor handling tug supply vessel. Appl. Energy 226, 423–436. http://dx.doi.org/10.1016/j.apenergy.2018.05.131.

Zis, Thalis P.V., Psaraftis, Harilaos N., Ding, Li, 2020. Ship weather routing: A taxonomy and survey. Ocean Eng. 213, 107697. http://dx.doi.org/10.1016/j.oceaneng.2020.107697.

Zou, H., Hastie, T., 2005. Regularization and variable selection via the elastic net. J. R. Stat. Soc. Ser. B Stat. Methodol. 67 (2), 301–320.

Zuurendok, Bastiaan, 2005. Advanced Fuel Consumption and Emission Modeling Using Willans Line Scaling Techniques for Engines. Technical Report, Technische Universiteit Eindhoven, Department Mechanical Engineering, Dynamics and Control Technology Group.